ISTANBUL TECHNICAL UNIVERSITY ★ INSTITUTE OF SCIENCE AND TECHNOLOGY

SEPARATION CONTROL BY STEADY AND UNSTEADY SUCTION

M.Sc. Thesis
A. TUNÇ, B.Sc.

Department: Aeronautical Engineering

Programme: National and International
Integrated Graduate Program
Special Program for the
Turkish Airforce Personnel

DECEMBER 2002

ISTANBUL TECHNICAL UNIVERSITY ★ INSTITUTE OF SCIENCE AND TECHNOLOGY

SEPARATION CONTROL BY STEADY AND UNSTEADY SUCTION

M.S. Thesis

Ali TUNÇ, B.Sc.

(511011021)

Date of Submission : 24 December 2002

Date of Defence Examination : 13 January 2003

Supervisor : Assoc. Prof. Dr. F. Oğuz EDİS (İ.T.Ü.)

Co-Supervisor : Prof. Dr. Osame KANDIL (O.D.U.)

Members of Committee : Assoc. Prof. Dr. Aydın MISIRLIOĞLU (İ.T.Ü.)

Assoc. Prof. Dr. İbrahim ÖZKOL (İ.T.Ü.)

JANUARY 2003

İSTANBUL TEKNİK ÜNİVERSİTESİ ★ FEN BİLİMLERİ ENSTİTÜSÜ

DAİMİ VE ZAMANA BAĞLI EMME İLE AKIM AYRILMASININ KONTROLÜ

YÜKSEK LİSANS TEZİ

Ali TUNÇ
(511011021)

Tez Teslim Tarihi : 24 Aralık 2002

Tez Savunma Tarihi : 13 Ocak 2003

Tez Danışmanı : Assoc. Prof. Dr. F. Oğuz EDİS (İ.T.Ü)

Eş-Danışman : Prof. Dr. Osama KANDIL (O.D.U)

Jüri Üyeleri : Assoc. Prof. Dr. Aydın MISIRLIOĞLU (İ.T.Ü)

Assoc. Prof. Dr. İbrahim ÖZKOL (İ.T.Ü)

OCAK 2003

ACKNOWLEDGEMENTS

I would like to express my sincere appreciation to my advisors Dr. Osama KANDIL, ODU and Dr. F. Oğuz EDİZ, ITU for their valuable guidance and support during the entire course of this study. I also would like to express my sincere gratitude to my committee members for their useful comments and suggestions during the dissertation preparation.

Special thanks are also extended to Dr. Alim Rustem Aslan for providing essential support in generating the computational grids. Their encouragement, assistance and friendship have also been of immense help in finishing this research. The moral and technical supports of research assistants and air force colleagues are also appreciated.

I would like to express my sincere respect for Turkish Air Force for choosing and providing the funding for the entire program.

Finally, I would like to take this opportunity to express my deepest love, appreciation, and gratitude to my family for their continuous support and encouragement.

Thank you very much.

Ali TUNC
December 2002

CONTENTS

LIST OF TABLES

LIST OF FIGURES

LIST OF SYMBOLS

a	: speed of sound
$\tilde{A}$	: Roe-Averaged Flux Jacobean Matrix
A_{ij}	: cell face area
AOA	: angle of attack
C_N	: normal force coefficient
C_D	: drag coefficient
C_L	: lift coefficient
C_p	: pressure coefficient
CFD	: computational fluid dynamics
CFL	: Courant-Friedrichs-Lewy number
CFL3D	: Computational Fluids Laboratory 3-Dimensional flow solver
CPU	: central processing unit
Cq	: mass flow flux
d	: diameter
DDT	: Domain Decomposition Technique
e	: total energy
e_0	: energy per unit volume
$\vec{E}$	: inviscid flux vector
FD	: Finite Difference
FDS	: Flux Difference Splitting
FV	: Finite Volume
FVS	: Flux Vector Splitting
$\vec{F}, \vec{G}, \vec{H}$	: flux vectors in cartesian coordinates
$\hat{F}, \hat{G}, \hat{H}$	: flux vectors in curvilinear coordinates
h	: enthalpy
h_0	: enthalpy per unit volume
J	: transformation Jacobean
k	: cell face
M_∞	: free stream mach number
n	: unit normal
$\hat{n}$	: outward facing unit normal
$\vec{N}$	: outward pointing normal to the boundary

p	: pressure
P	: static pressure
Q	: conserved variables
$\vec{Q}$	: conserved variables in vector form
$\hat{Q}$	: conserved variables in curvilinear coordinates
Q_L	: conserved variables to the left of the interface
Q_R	: conserved variables to the right of the interface
R_i	: residual
$R^{\pm}$	: Riemann invariants
t	: time
T	: temperature
u, v, w	: velocities in cartesian coordinates
U, V, W	: contravariant velocities
$\vec{V}$	: velocity vector
V_i	: volume
x, y, z	: cartesian coordinates of grids
α	: angle of attack in degree
$\tilde{\Gamma}$	: right eigenvectors of Roe-averaged flux Jacobean matrix
$\tilde{\Gamma}^{-1}$	: left eigenvectors of Roe-averaged flux Jacobean matrix
γ	: ratio of specific heats
ρ	: density
ξ, η, ζ	: generalized curvilinear coordinates
$\Delta_{\pm}$	: forward and backward differencing
Λ	: diagonal matrix
Δ	: change

SEPARATION CONTROL BY STEADY AND UNSTEADY SUCTION

SUMMARY

The effectiveness of combat aircraft depends in part on their ability to maintain high lift under extreme conditions. Examples of such conditions include the high angle of attack, rapid pitch motions necessary for combat maneuvers. A well-known phenomena occurring on airfoils undergoing such high angle of attack motions is the formation of a leading vortex. This vortex proceeded by significant increase in lift, but it is also accompanied by subsequent rapid loss of lift and the ensuring dynamic stall.

New type aircrafts have high cruise speed. Increase at cruise speed causes decrease at wing area and increases at landing speed. There is a relation between landing speed and landing distance. If the landing speed increases, landing distance also increases. To decrease landing distance aircraft need high angel of attack during landing. This also cause dynamic stall.

In past years, many experimental and numerical studies have been devoted to improve the aerodynamic characteristics of the dynamic stall, thereby to enlarge flight envelope. All of such efforts can be roughly categorized as being either passive or active control measure to meet the goals.[1-2] Passive techniques are characterized by fixed devices that are configured to improve system performance. Active control strategies are based on the idea that the onset of flow separation might be delayed by directly supplying kinetic energy into the boundary layer, enhancing the turbulent entrainment rate. Many experimental and numerical studies are conducted to solve separation problem.

In this study, a numerical study was conducted to investigate effects of fixed unsteady and steady suction on a modified NACA0012 airfoil. The fixed unsteady suction was applied on airfoil. Flow field predictions are made using a modified version of the CFL3DV(5) unsteady, two-dimensional, compressible Navier-Stokes solver. C type grid was used.

Suction is applied to surface with an angle to surface normal. The effect of suction is investigated. Numerical results are obtained at M=0.3 and 12 and 15 degrees angle of attack with one suction section and with two suction section. At first flow is solved for No- control at M=0.3 and 12 and 15 degrees angle of attack. Cp diagrams were used to predict suction location. Steady suction is applied at leading edge. This case gave us good results. Separation point moved forward on airfoil. This steady control case also gave us where to apply second suction location. Unsteady suction was applied at two locations on airfoil. Suction frequency was obtained from lift history by solving fast furrier series from no-control case. After applying suction at two locations, separation is nearly controlled.

Our numerical solutions have indicated that unsteady suction, with the careful selection of peak amplitude, frequency and location; enhance the lift characteristics

of airfoil. The unsteady suction can be use as a mean of separation control to generate lift on airfoils.

ÖZET

Savaş uçağının etkinliği zor şartlarda yüksek kaldırma üretme yeteneğine bağlıdır. Yüksek hucum açılarını ve ani savaş manevralarını bu zor şartlara ornek olarak verebiliriz. İyi bilinen olay yüksek hücum açılarında oluşan hücum kenarı vorteksi dir. Bu vortex kaldırmadaki belirgin bir artışla başlar fakat kaldırmadaki ani düşüş bunu takip eder ve sonunda dinamik stall oluşur.

Yeni tip uçaklar yüksek seyir süratlerine sahiptir. Seyir süratlerinde ki artış kanat alnalarında azalma ve iniş süratlerinde artışa sebeb olur. İniş hızı ile iniş mesafesi birbiri ile ilişkilidir. İniş hızının artması iniş mesafesinin artmasının sebep olur. İniş mesafesini azaltmak ancak yüksek hücum açısıyla mümkün olur buda dinamik stala sebep olur.

Geçmiş yıllarda bir çok deneysel ve sayısal çalışma dinamik stalun aerodinamik karakteristiklerini geliştirmek ve bu sayededе uçuş alanını geliştirmek için yapılmıştır. Bütün bu çalışmalar pasif ve aktif olmak üzere iki kategoriye ayrılabılır. Pasif teknikler, sistemin performasını arttırmak amacıyla tasarlanmış araçlardır. Actif kontrol stratejisi ise akım ayrılmasının sınır tabakasına enerji ilave etme fikrine dayanır. Akım ayrılması problemini çozmek için bir çok sayısal ve deneysel çalışma yapılmıştır..

Bu çalışmada, daimi ve daimi olmayan şekilde akımın emilmesinin modife edilmiş NACA0012 profiline olan etkilerinin hesaplamalı analizi yapılmıştır. Kanadın üstünde iki bolgede hava akımı emilmiştir. Akım alanı tahminleri NASA'nın kullandığı, daimi olmayan, iki boyutlu, şıkıştırılabilir Navier-Stokes denklemelrini kullnanan CFL3DV(5) programıyla yapılmıştır. Ctipi grid kullanılmıştır.

Hava akımı yüzey normeline gore belli bir açıyla emilmiştir. Sayısal çalışmalar 0.3 Mach sayısında 12 ve 15 derece hucum açısında yapılmıştır. İlk once 0.3 Mach sayısında 12 ve 15 derecede konrol uygulamadan akımalanı tahminlerini yaptık. Cp diagramlarını hava akımını emeceğimiz yeri belirlemek için kullnadık. Hücum kenarıda bir bolgede daimi bir şekilde hava akımını belli bir oranda emdik(suction). Ayrılma noktasının profilin üst tarafına doğru ilerlediğini gozlemledik. Bu durum ayriça ikinci suction bolgesini nereye uygulayacamızı bulmada yardımcı olmuştur. Profil üzerinde iki bolgede daimi olamayan suction uyguladık. Suction frekansını kontrol uygulmadığımız durumdaki kaldırma değişimlerini Fast Fourier serileriyle çozerek elde ettik. İki bolgede suction uyguladiktan sonra akımayrılmasının kısmen kontrol edildiğini gozlemledik.

Yaptığımız çalışmalar göstermiştirki; daimi olmayan birşekilde kanat üstünden akımın emilmesi, emme oranin, frekansinin ve yerinin dikkatli bir şekilde seçimiyle, kaldırma üzerinde onemli etkileri olmuştur. Daimi olamayan bir şekilde kanat üstünde hava akımının çekilmesi akım ayrılmasının kontrolünde ve profillerde taşımayı arttırmak için kullanılabilir.

1. INTRODUCTION

1.1 Motivation

Combat aircrafts have to maintain high lift under extreme conditions such as the high angle of attack or rapid pitch motions necessary for air combat maneuvers. The leading edge vortex is occurring under such high angle of attack motions. This vortex is preceded by significant increase in lift, but it is also accompanied by subsequent rapid loss of lift and ensuring dynamic stall. [1, 2]

Aircraft has to have maneuverability and stability to perform in combat situations. Design changes in air-to-air weapons have increased the need for fighter-aircraft to execute difficult maneuvers. Turning performance is an example for this. The development of all-aspect short-range infrared guided missiles and all aspect guns caused some improvements aircrafts performance [1, 2]

New type aircrafts have high cruise speed. If the cruise speed increases wing area decreases and landing speed increases. There is a relation between landing speed and landing distance. If the landing speed increases landing distance increases also. To decrease landing distance aircraft need high angle of attack during landing. This also cause dynamic stall.

These post- stall regime maneuvers utilize thrust control to achieve rapid attitude changes. Such conditions may result in unsteady separation on wing. This situation can lead to increased drag, wing buffeting, and stability and control problems, which degrade, combat effectiveness and could cause the loss of the aircraft. [3]

During forward or maneuvering flight of helicopters, the angle of attack of the rotor blade sections periodically changes and reaches large values as the blade rotate and pass through the so called retreating blade position. On an airfoil whose incidence is increasing rapidly, the onset of the stall can be delayed to incidences, which may exceed the static stall angle, by a significant amount. However, once dynamic stall occurs, the aerodynamic loads are generally more severe and may cause significant increase in the blade stresses and the control system loads. Therefore, dynamic stall limits the helicopter flight envelope and methods are required to predict its occurrence.

Dynamic stall also occurs on horizontal axis wind turbines, where rather complex blade incidence variations are generated by the unsteady inflow conditions due to atmospheric turbulence and during operation in yaw. Dynamic stall also may be encountered on propeller and turbo machinery blades and on the wings of rapidly and wings of rapidly maneuvering fighter aircraft and missiles. [4]

1.2 Separation and point of separation

In order to explain the separation let consider the flow on airfoil at an angle of attack, such as shown in Figure 1.1. The flow accelerated from A (stagnation point) to B and decelerated from A to C. Hence, pressure decrease from A to B and increase from A to C. While a particle is moving from A to C, it loses its kinetic energy due to viscous forces. The point of separation is defined as the limit between forward and reverse flow in the layer in immediate neighborhood of the wall or point of separation: $\left(\frac{\partial u}{\partial y}\right)_{wall} = 0$

Figure 1.2 shows a representation of flow in boundary layer. Figure 1.3 shows the separated flow on airfoil.

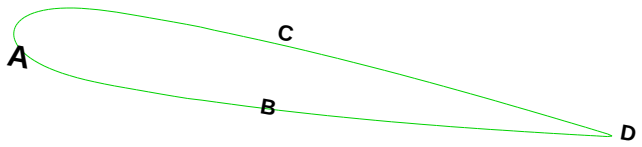

Figure 1.1 Airfoil

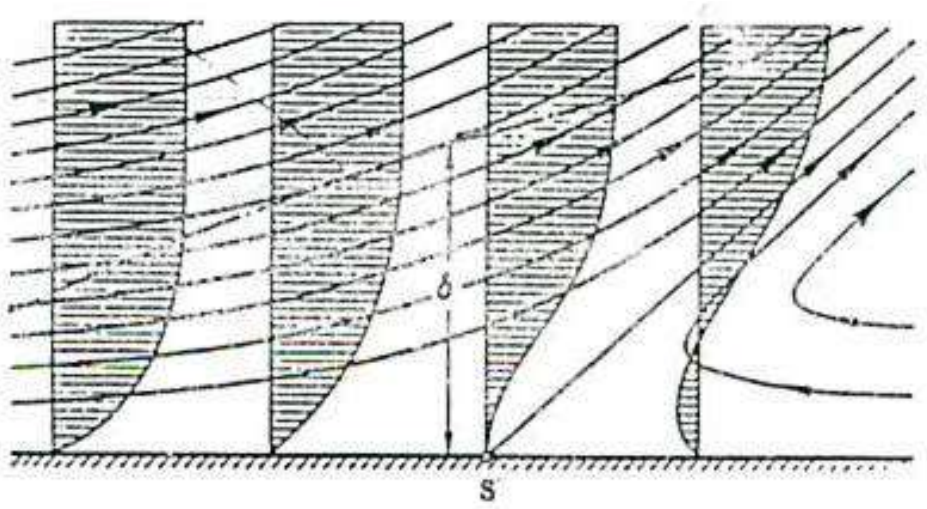

$$\left(\frac{\partial u}{\partial y}\right)_{wall} < 0 \qquad \left(\frac{\partial u}{\partial y}\right)_{wall} < 0 \qquad \left(\frac{\partial u}{\partial y}\right)_{wall} = 0 \qquad \left(\frac{\partial u}{\partial y}\right)_{wall} < 0$$

Figure 1.2 Diagrammatic representation of flow in the boundary layer (Reproduced from [5]).

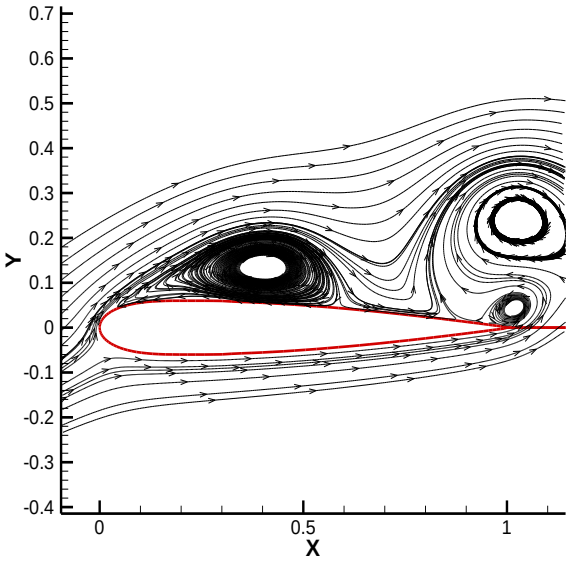

Figure 1.1 Separated flow on an airfoil

1.3 Literature Survey

In past years many experimental and numerical studies have been devoted to improve the aerodynamic characteristics of the dynamic stall, thereby to enlarge flight envelope. All of such efforts can be roughly categorized as being either passive or active control measure to meet the goals. [6, 7] Fixed devices that are configured to improve system

performance characterize passive techniques. Passive control devices are simple, and relatively low in cost but there are some significant disadvantages. They cannot be controlled and add parasitic drag in situations where suppression is not needed. Passive control methods are intrinsically unable to adjust to changing flowfields. [8] Because of this, the active control methods have attracted more interest recently. Unlike passive control methods, active control strategies are based on the idea that the onset of flow separation might be delayed by directly supplying kinetic energy into the boundary layer, enhancing the turbulent entrainment rate. Active techniques have the potential to minimize both disadvantages while optimizing overall performance. Conceptually, active control methods can be divided into two categories, one for stationary and the other one for moving control devices. [6] Thus for blowing, [9, 10] suction, [11, 12] oscillatory surface heating [13], and acoustic excitation [14] have been suggested for motionless devices. Examples in which motion of the control device is employed are moving surface, [15] buzz, [16] thickness variation [17], oscillating flap, [8, 18] and deformable leading edge. [6, 19, 20]

Chandrasekhara [21] made an experimental investigation of the unsteady effects of dynamically deforming the leading edge of an airfoil. He found that by carefully selecting a fixed shape for the leading edge geometry, the dynamic stall vortex was completely eliminated.

Sahin and Sankar [22] made a numerical investigation, based on Chandrasekhara's work [21], about dynamic stall control using a deformable leading edge and they found that dynamic deformable leading edge (DDLE) airfoils had a slightly dynamic stall behavior compared to NACA0012 airfoil.

Kehro and Hutcherson used a fixed vortex generator on high-lift systems. At landing/takeoff conditions, the vortex generator transports high momentum fluid from the boundary layer towards the wing surface, energizing the boundary layer and delaying separation. Thus lift is increased and performance loses are reduced. [18]

Geissler and Raffel have studied the feasibility of dynamic stall control via active thickness variation by means of dynamic stall control via active thickness variation by means of numerical analysis and experiments [16]. The research results showed that the

overall aerodynamics characteristics are greatly influenced by the strategies of the thickness variation. The concept of thickness variation is relatively simple and has an advantage of increasing the maximum lift without invoking the earlier drag divergence and moment stall. [17]

Ramsey and Thomas [19] used a periodic blowing and suction normal to surface at 2.5% chord from the leading edge of NACA0012 airfoil. They showed that lift was increased for angles of attack between 18^0 and 35^0. They used the Reynolds average Navier-stokes (RANS) approach with the Baldwin-Lomax algebraic turbulence model.

Hassan and Janakiram [19] have also used RANS approach with Baldwin–Lomax Turbulence model. In their work zero net mass suction/blowing was placed at 13% chord and they found that for certain oscillation frequency and peak amplitude, the lift can be increased albeit with high momentum input. The comparison with experiments was not given in both articles.

Donovan, Linda D. Janakiram [23] made a numerical investigation both steady and unsteady jet on airfoils. They used an unsteady RANS incompressible flow solver with Spalart Allmaras turbulence model and compared their results with the experiments of Seifert and Bachar. [24]

Ravindran [25] made a numerical investigation of unsteady suction and blowing on an airfoil using a compressible flow solver CFL3D. He builds a previous work of Donovan [23] to validate CFL3D for active flow control applications. He used Spalart Allmaras turbulence model. He found that the lift increased as the blowing coefficient increased.

Karim and Acharya [26] developed a strategy for altering the unsteady flow development and the formation of the dynamic-stall vortex. Their approach was to control the accumulation of reverse-flow fluid in the leading edge region of the airfoil suction surface by removing fluid at a specified rate through a suction slot located in the suction surface near the leading edge, at about 2% of chord.

1.4 Comparison between Steady and Unsteady Separation

There is a difference between the two separation mechanisms. In steady separation, the flow is sufficiently retarded due to adverse pressure gradient, and the momentum of the fluid particles is reduced. The retarded particles cannot penetrate into the high-pressure region due to their reduced kinetic energy. The boundary layer is deflected away from the wall and separates from it. The point of separation is defined as the point where the wall shear vanishes [27]. In unsteady separation, the separation point does not necessarily coincide with the point of vanishing wall shear [28]. Rather, the unsteady separation point is determined by the simultaneous vanishing of the wall shear and the profile velocity at a point just above the wall as seen by an observer moving with the separation velocity [29]. This is known as the MRS criterion. If the observer is fixed at a point on the airfoil surface, it is possible to observe zero velocity or zero shear stress and not have unsteady separation. An abrupt thickening of the boundary layer causes the separation, which result in the retarded fluid in the boundary layer being ejected into the potential flow

1.5 Characteristics of the Steady Airfoil Flows

In our calculations steady airfoil is used. There are three specific types of stall [30]. The first is leading edge stall, where the flow separation initially near the leading edge but reattaches almost immediately due to rapid transition to turbulence. This reattachment occurs when the pressure nearly equals the value that would exist if the boundary layer was turbulent and attached [31]. This region between separation and reattachment is comparable in size to the thickness of the boundary layer. As the stall angle is approached, the region grows shorter until the adverse pressure gradient results in airfoil separation. The separation/reattachment region is significant because it determines the initial conditions of the boundary layer downstream. It is the type of stall, which occurs on a static airfoil. According to Lissaman [32], the region between separation and reattachment, known as a laminar separation bubble, occurs only on airfoils below a chord Reynolds number of 50,000. Above this point, the airfoil is physically too short for reattachment to occur.

The second type of stall, thin-airfoil stall, is characterized by laminar flow separation at the airfoil leading edge and coinciding reattachment at some point downstream. The reattachment location moves downstream along the airfoil surface as the angle of attack is increased, creating what is known as a long separation bubble. This concept will be elaborated on in a letter section.

The third kind of stall is trailing edge stall, which involves the forward movement of a turbulent separation point from the trailing edge. This kind of stall occurs on unsteady airfoils.

For all Reynolds numbers, the flow over a static airfoil separates at a sufficiently high angle of attack. At Reynolds numbers below about 100,000 extensive separations on the upper airfoil surface may be possible even at low angles of attack. For these cases, the laminar boundary layer fails to overcome the adverse pressure gradient and separates, forming an unattached free shear layer. According to Mueller and Batil [30], the lift and drag on a static airfoil increase as Reynolds Number increases. The angle of attack corresponding to airfoil stall also increases, but only slightly. [33]

In this study, a numerical investigation of unsteady suction on an airfoil using flow solver CFL3D (V5) is presented. Suction is applied to surface with angle to surface normal on a modified NACA0012. CFL3D (V5) Boundary conditions are changed to apply suction with an angle. Numerical results are obtained at M=0.3 and 12 and 15 degree angle of attack. In this study effects of suction location and amplitude are also showed.

2. MATHEMATICAL MODEL AND COMPUTATIONAL ALGORITHM

2.1 Flow Dynamics Equations

The dimensionless, unsteady, compressible Navier-Stokes equations in conservative form are given by

$$\frac{\partial \overset{\varpi}{Q}}{\partial t} + \frac{\partial \overset{\varpi}{E}_j}{\partial \xi_j} = \frac{\partial (\overset{\varpi}{E}_v)_j}{\partial \xi_j}, \qquad j = 1, 2, 3 \tag{2.1}$$

The flowfield vector $\overset{\varpi}{Q}$, inviscid flux $\overset{\varpi}{E}_j$ and viscous flux $(\overset{\varpi}{E}_v)_j$ are given by

$$\overset{\varpi}{Q} = \frac{Q}{J}$$

$$\overset{\varpi}{E}_j = \frac{1}{J}\left((\xi_j)_t Q + (\xi_j)_k E_k\right)$$

$$(\overset{\varpi}{E}_v)_j = \frac{1}{J}(\xi_j)_k (E_v)_k$$

(2.2)

$$J = \frac{\partial(\xi_1, \xi_2, \xi_3, t)}{\partial(x_1, x_2, x_3, t)}, \quad Q = \begin{bmatrix} \rho \\ \rho u_1 \\ \rho u_2 \\ \rho u_3 \\ \rho e \end{bmatrix},$$

$$E_k = \begin{bmatrix} \rho u_k \\ \rho u_1 u_k + \delta_{1k} p \\ \rho u_2 u_k + \delta_{2k} p \\ \rho u_3 u_k + \delta_{3k} p \\ \rho u_k (e + \frac{p}{\rho}) \end{bmatrix}, \quad (E_v)_k = \begin{bmatrix} 0 \\ \tau_{k1} \\ \tau_{k2} \\ \tau_{k3} \\ u_n \tau_{kn} - q_k \end{bmatrix} \tag{2.3}$$

Where Q is the flow vector in the Cartesian coordinates, and J is the Jacobian of the transformation from the Cartesian coordinates to the body-conformed coordinates. E_k are the inviscid flux vectors in Cartesian coordinates and $(E_v)_k$ are viscous and heat conduction fluxes vectors in Cartesian coordinates. 2.3 give them

Where τ_{kn} is the shear stress tensor. For Newtonian fluids with the Stokes's hypothesis, $\lambda = -\frac{2}{3}\mu$, τ_{kn} is given by

$$\tau_{kn} = \frac{\mu M_\infty}{Re}\left(\frac{\partial u}{\partial x_n} + \frac{\partial u_n}{\partial x_k} - \frac{2}{3}\delta_{kn}\frac{\partial u_m}{\partial x_m}\right) \tag{2.4}$$

And the heat conduction flux, q_k, is given by

$$q_k = \frac{-\mu M_\infty}{(\gamma - 1)\,Pr\,Re}\frac{\partial T}{\partial x_k} \tag{2.5}$$

The variables in Equations are non-dimensionalized by using the reference parameters. The reference parameters are $L, a_\infty, L/a_\infty, \rho_\infty$ and μ_∞ for the length, velocity, time, density and molecular viscosity, respectively. The pressure is non-dimensionlized by $\rho_\infty a_\infty^2$. The free stream Reynolds number is defined by $Re = \frac{\rho_\infty U_\infty L}{\mu_\infty}$ and the Prandtl number, $Pr = \frac{\mu C_p}{k}$, is chosen as 0.72. Sutherland's law gives the dimensionless viscosity

$$\mu = T^{\frac{3}{2}}\left(\frac{1+c}{T+c}\right) \tag{2.6}$$

Where T is the non-dimensional temperature and c is the Sutherland's constant, $c \approx 110.4/T_\infty$.

2.2 Finite Volume Formulation: Roe's Upwind Scheme

The conservative form of the full Navier-Stokes equations, Eqn. 2.1, can be integrated over the domain V

$$\int_v \frac{\partial \vec{Q}}{\partial t} dv + \int_v \frac{\partial (\vec{E}_j - (\vec{E}_v)_j)}{\partial \xi_j} dv = 0 \qquad (2.7)$$

Applying the Gauss divergence theoremt o the second term, the equation above can be rewritten as

$$\int_v \frac{\partial \vec{Q}}{\partial t} dv + \oint_{\partial \Re} \frac{\vec{E}_j - (\vec{E}_v)_j}{J} \vec{a}_m \cdot \hat{n} \, ds = 0 \qquad (2.8)$$

Where $\vec{a}_m$ is the covariant base vector, $\partial \Re$ the boundary enclosing computational domain V and $\hat{n}$ the unit outward normal of $\partial \Re$

2.2.1 Roe's Flux-Difference Splitting

The flux-difference splitting scheme developed by Roe is based on a characteristics decomposition of the flux differences. Roes scheme posses the conservation properties. Consider the one-dimensional equation

$$\frac{\partial Q}{\partial t} + \frac{\partial E}{\partial x} = 0 \qquad (2.9)$$

Where E is a function of first order of Q Using the chain rule, this equation can be written as

$$\frac{\partial Q}{\partial t} + A \frac{\partial Q}{\partial x} = 0 \qquad (2.10)$$

Where $A = \frac{\partial E}{\partial Q}$ is the flux Jacobian matrix. The exact solution of the Riemann problem can be written as

$$E_R - E_L = \sum_i \alpha_i \lambda_i e_i \qquad (2.11)$$

Where α_i represents the projection of the difference in Q between the initial right and left states, λ_i and e_i are the eigenvalues and eigenvectors of the Jacobian matrix A, respectively. The interface flux can be determined using

$$E_{j+\frac{1}{2}}(Q_L, Q_R) = \frac{1}{2}\left(E_L + E_R - \sum_{i=1}^{3} \alpha_i \lambda_i e_i \right) \qquad (2.12)$$

Consider the Euler equations, where E is not a linear function of Q. Roe suggested the following form

$$\frac{\partial Q}{\partial t} + \overline{A}\frac{\partial Q}{\partial x} = 0 \qquad (2.13)$$

Where $\overline{A}$ is the Roe-average matrix, which satisfies the following conditions:

1. $\overline{A}$ Constitutes a linear mapping from the vector space Q to the vector space E.
2. As $Q_L \to Q_R \to Q$, $\overline{A}(Q_L, Q_R) \to A(Q)$
3. For any Q_L and Q_R, $\overline{A}(Q_L, Q_R) \times (Q_L - Q_R) = E_L - E_R$
4. The eigenvectors of $\overline{A}$ are linearly independent.

Based on the third property, the flux difference between the left and right states and the interface fluxes can be written as

$$E_R - E_L = A(Q_L - Q_R) \qquad (2.14)$$

$$E_{j+\frac{1}{2}}(Q_R - Q_L) = \frac{1}{2}\left[(E_L + E_R) - \left|\overline{A}\right|(Q_R - Q_L) \right]_{j+\frac{1}{2}} \qquad (2.15)$$

The last term of Eq. 2.15 is the dissipation term.

2.3 Initial and Boundary Conditions

The solution of any partial differential equation is completely depending on the choices of initial and boundary conditions. The initial conditions should correspond to the physical nature of the flow. As it is expected, different form of such conditions must be used for steady and unsteady calculations.

Two types of boundary condition representations are employed in CFL3D, namely, cell-center and cell-face. For cell-center type boundary conditions, the flow field variables are specified at "ghost" points corresponding to two cell center locations analytically extended outside the grid. For cell-face type boundary conditions, the flow field variables and their gradients are specified at the cell face boundary.

As the initial conditions, the free stream Mach number of 0.3 and the free stream temperature of 460 degrees Kelvin are applied for all the cases.

Extrapolation boundary conditions are cell-center type boundary conditions. The ghost points are extrapolated from the computational domain. Based on the locations of ρ_1, ρ_{-1} and ρ_{-2} (Figure 2.1) the extrapolated values would be

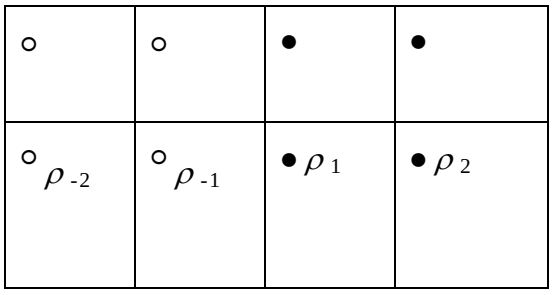

Figure 2.1 Extrapolated Points

$\rho_{-1}=\rho_1$ and $\rho_{-2}=\rho_1$

The free stream boundary conditions are cell-center type boundary conditions. The flow field variables for both sets of ghost points are set equal to the initial values, which are:

$$\rho_{initial} = 1.0 \qquad (2.16a)$$

$$u_{initial} = M_\infty \cos\alpha \cos\beta \qquad (2.16b)$$

$$v_{initial} = -M_\infty \sin\beta \tag{2.16c}$$

$$w_{initial} = M_\infty \sin\alpha\cos\beta \tag{2.16d}$$

$$p_{initial} = \rho_{initial}\left(a_{initial}\right)^2/\gamma \tag{2.16e}$$

It should be noted that all boundary conditions used in this study are specified explicitly. The walls are considered impermeable and adiabatic. Using locally one-dimensional characteristic boundary conditions incorporates the far field boundary conditions. The velocity normal to the boundary and the speed of sound for each cell are calculated from the locally one-dimensional Riemann invariants, that is

$$R^{\pm} = U \pm \frac{2}{\gamma - 1}a \tag{2.17}$$

The invariants, for example in ξ direction, are constant along the characteristics defined as

$$\left(\frac{d\xi}{dt}\right)^{\pm} = U \pm a \tag{2.18}$$

These invariants are used to calculate the local normal velocity and the speed of sound. Adding or subtracting the two Riemann invariants respectively calculates the local normal velocity and the speed of sound at the boundaries. The local normal velocity is calculated by summing and the speed of sound is calculated by subtracting them. Other quantities such as density and pressure can be found by using the entropy relation and the equation of state respectively. For steady inviscid flows, the velocity components used in the surface boundary conditions and the contravariant velocity, which is U, can be expressed as

$$u_{wall} = u_{center} - n_x U \tag{2.19a}$$

$$v_{wall} = v_{center} - n_y U \tag{2.19b}$$

$$w_{wall} = w_{center} - n_z U \tag{2.19c}$$

$$U = \vec{V} \bullet \hat{n} = un_x + vn_y + wn_z \qquad (2.20)$$

The entropy is determined using the value from outside the domain for the inflow and from inside the domain for outflow. The entropy and speed of sound are used to determine the density and pressure on the boundary. The pressure for the boundary conditions can be obtained by extrapolation from the interior point value that is order of zero. The density is then calculated by employing the state equation [40, 41]. The outer boundary conditions of the grids are shown in the figure 2.1 and 2.2.

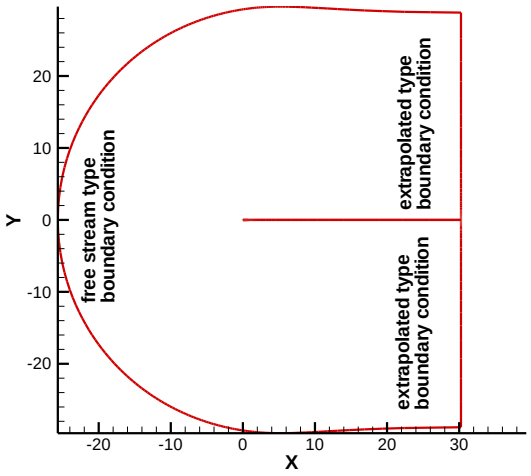

Figure 2.1: Outer Boundary Conditions

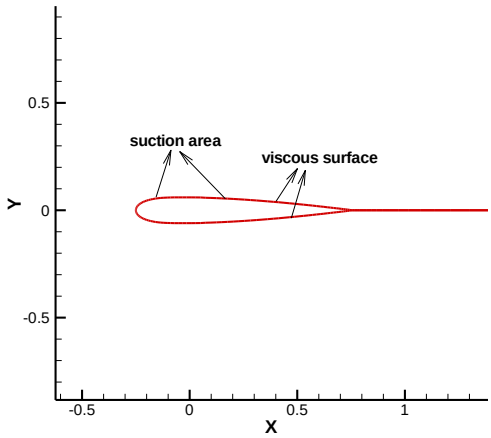

Figure 2.2: Surface Boundary Conditions

The viscous boundary conditions are cell-face type boundary conditions. Two pieces of auxiliary information are supplied on input: the wall temperature (T_w/T_∞) and mass flowrate (Cq), where Cq=(ρu_{normal})/(ρu)

The surface velocities are the determined as

$$U_w = M_\infty \; Cq \, \xi_x \Big/ |\nabla \xi| \cdot \frac{(c2)}{\gamma Pb} + umesh \qquad (2.21)$$

$$v_w = M_\infty \; Cq \, \xi_y \Big/ |\nabla \xi| \cdot \frac{(c2)}{\gamma Pb} + vmesh \qquad (2.22)$$

$$w_w = M_\infty \, Cq \, \xi_z / |\nabla \xi| \cdot \frac{(c2)}{\gamma Pb} + w_{mesh} \qquad (2.23)$$

u_{mesh}, v_{mesh}, w_{mesh} are the velocity components of the mesh. In this study they are equal to zero because the mesh is not in motion.

This type boundary condition allows applying suction. Some changes on boundary condition of CFL3D made to apply suction with an angle to surface normal.

3. COMPUTATIONAL ALGORITHM

3.1 About Cfl3D

Predictions were made using a modified version of the NASA CFL3D (v5), a Reynold-Avaraged thin-layer Navier-Stokes flow solver for structured grids. The original version of CFL3D was developed in the early 1980's in the Computational Fluid Laboratory at NASA Langley Research Center; hence the name of the code, which is an acronym for the Computational Fluids Laboratory 3-Dimensional flow solver. An overview of the history of the code can be found in Rumsey, Biedron, and Thomas. [32]

CFL3D solves the time dependent conservation law form of the Reynolds-Averaged Navier-Stokes equations. The spatial discretization involves a semi-discrete finite-volume approach. Upwind biasing is used for the convective and pressure terms, while central differencing is used for the shear stress and heat transfer terms. Time advancement is implicit with the ability to solve steady or unsteady flows. Multigrid and mesh sequencing are available for convergence acceleration. Numerous turbulence models are provided, including 0-equation, 1-equation, and 2-equation models. Multiple-block topologies are possible with the use of 1-1 blocking, patching, overlapping, and embedding. CFL3D does not contain any grid generation software. Grid must be supplied extraneously.

Version 5.0 of CFL3D has several additional utilities over earlier version of the code. Most notably, Version 5.0 has the capability to employ sliding patched-zone interfaces, such as might be required to perform rotor-stator computations, for example. However, it is stressed here that CFL3D has been developed primarily as a tool for external aerodynamics analysis. Its use for internal turbo machinery applications has been only as a basic research code thus far; other Navier-Stokes codes specifically designed for turbo machinery applications, such as ADPAC, UNCLE TURBO, or ROTOR may be better suited to the analysis of such flows.

CFL3D does not have capability to solve unsteady-tangential suction/blowing. For this purpose boundary condition section of the code is chanced.

In our calculations Laminar flow condition and Roe's flux difference splitting scheme are used.

3.2 Grid

Computations were preformed on a C-type mesh having a resolution of 209x97. Figure one describes the computational grid generated for NACA-0012 airfoil. Hyperbolic grid-gen was used to generate the computational grid while enforcing grid orthogonality at the surface of the airfoil. Grid clustering was performed near the surface of the airfoil to resolve the details of the boundary layer. In the computational grid, the first grid points of the airfoils were located at a distance equal to 0.00001C. The far field boundary was located at a distance approximately equal to 30 airfoil chord lengths.

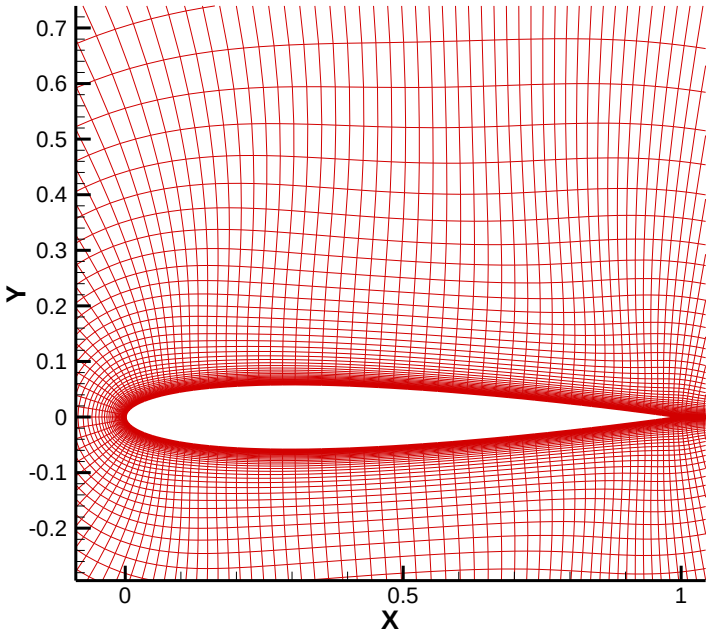

Figure 3.1.a Computational C-type grid around the airfoil

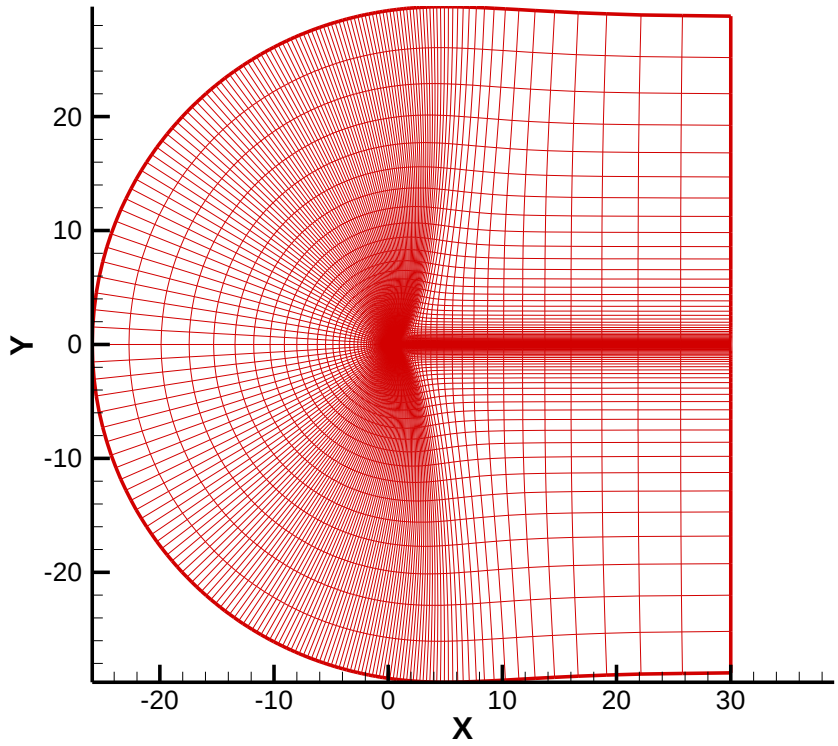

Figure 3.1.b Computational C-type grid around the airfoil

4. RESULTS

4.1 Cases

Six calculations for modified NACA0012 airfoil are performed. All calculations are done at Mach number 0.3. Three calculations are performed at 12 degree of angle of attack and three calculations are done at 15 degrees of angle of attack. First, flow predictions for 12 and 15 degree of angle of attack are done at Mach number 0.3 without any control applied. C_p and lift and drag history diagrams are used to predict suction location, frequency, and amplitude. Two control calculations for both 12 and 15 degree of angle of attack are done. At first one steady suction area near leading edge is applied. After that, calculation of second unsteady suction areas on airfoil applied. Table 4.1 shows these cases.

Table 4.1 Test Cases Showing Angle Of Attack, Control Type And Number Of Suction Area.

Mach number	Angle of attack	Control type	Number of suction area	
0.3	12	No-Control	-	
0.3	12	Steady control	1	
0.3	12	Unsteady control	2	
0.3	15	No-Control	-	
0.3	15	Steady control	1	
0.3	15	Unsteady control	2	

At 12 degrees of angle of attack steady suction is applied near leading edge. Suction location and suction amplitude are shown at figure 4.1. This case is called as steady suction. This case helps us to determine where to apply second suction area. Cp diagrams used to find the second suction area. Lift history at without control case used to find suction frequency. At 12 degree of attack unsteady two suction areas applied on

airfoil. Suction locations and suction frequency and amplitudes are shown at Figure 4.2. This case is called as unsteady suction.

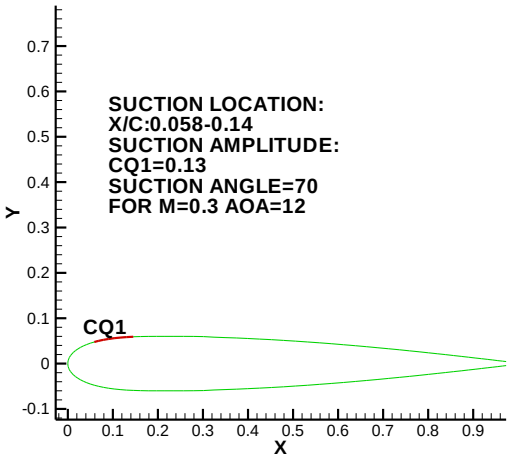

Figure 4.1 Suction Location and Amplitude for Steady Suction for M=0.3 at 12 Degree of Angle of Attack

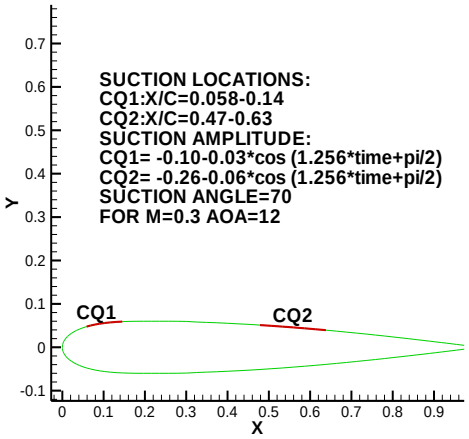

Figure 4.2 Suction Location and Suction Frequency and Amplitude for Unsteady Suction for M=0.3 at 12 Degree of Angle of Attack

At 15 degree of angle of attack same way was followed. First steady suction at one location is applied and using this case's results unsteady second suction area is applied. Figure 4.3 shows the suction location and amplitude for steady suction. Figure 4.4 shows the suction locations, suction frequency and suction amplitude for unsteady case.

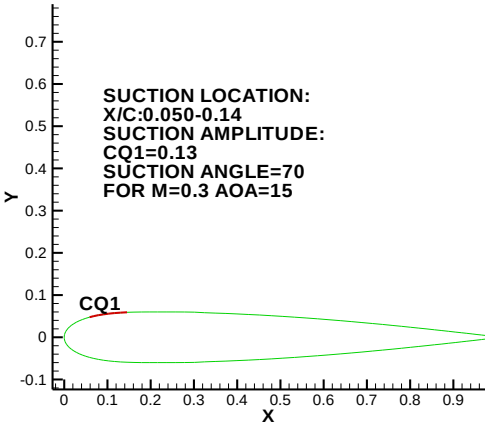

Figure 4.3 Suction Location and Amplitude for Steady Suction for M=0.3 at 15 Degree of Angle of Attack

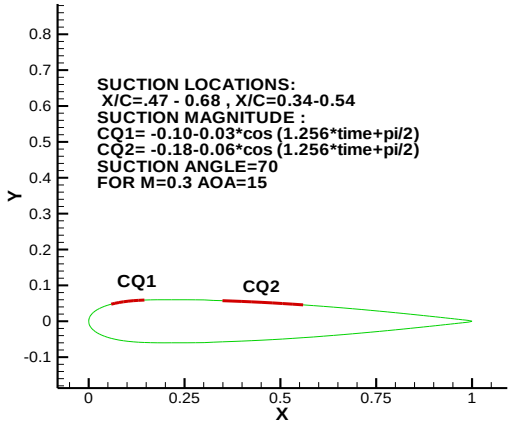

Figure 4.4 Suction Location, Suction Frequency and Amplitude for Unsteady Suction for M=0.3 at 15AOA

At all cases suction is applied with angle to surface normal.

Figure 4.5 shows the suction angle.

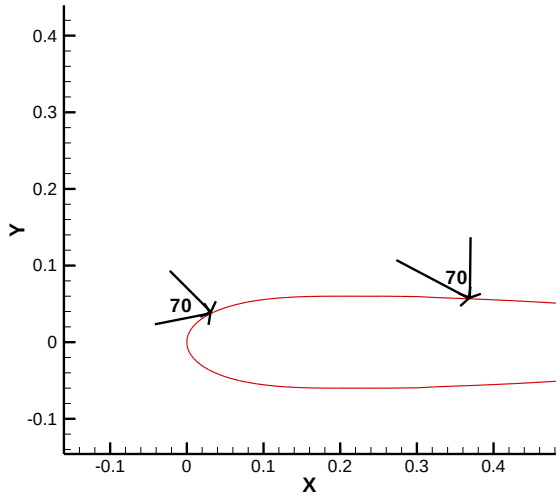

Figure 4.5 Suction Angle

4.2 Calculations for 12 Degree Of Angle Of Attack

4.2.1 Flow Predictions for Mach number 0.3 at 12 Degree of Angle Of Attack

At first flow predictions for Mach number 0.3 is made at 12 degree of angle of attack. Δt was obtained as $5x10^{-3}$, and fixed for all the following computations. The computations were extended to 20000 number of time step which is equivalent to non-dimensional time of T=100.

Figure 4.6 shows the time history of the lift and drag coefficient. The figure 4.6 shows oscillations. Except for transient time (0-4500 number of time step), the lift coefficient shows larger amplitude oscillations than drag coefficient. The maximum lift coefficient is 1.13 and the minimum lift coefficient is 0.63. The maximum drag coefficient is 0.25 and the minimum drag coefficient is 0.13. Oscillations at the lift and drag coefficient is unsteady and it is not possible to obtain an exact frequency. The continuous oscillations of the lift and drag coefficient is mainly due to the unsteady separation.

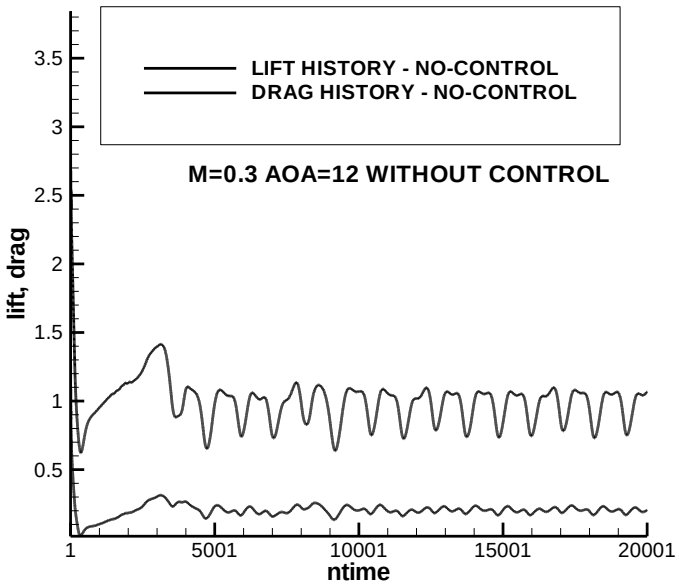

Figure 4.6 Time History of Lift and Drag Coefficient, M=0.3, AOA=12, Without Control

Figure 4.7 shows the eight-dimensional snapshot views of the streamlines at several time instants. The unsteady separation development is clearly observed. As the time goes separation starts near the leading edge and develops into a strong unsteady separated flow. Figure 4.8 shows the Mach Contours at different time instants. The development of unsteady separation can be seen. Figure 4.9 shows the C_p coefficient at several different time instants. C_P coefficient shows that separation is unsteady. The peak point of CP coefficient shows the separation location. Separation location differs in time.

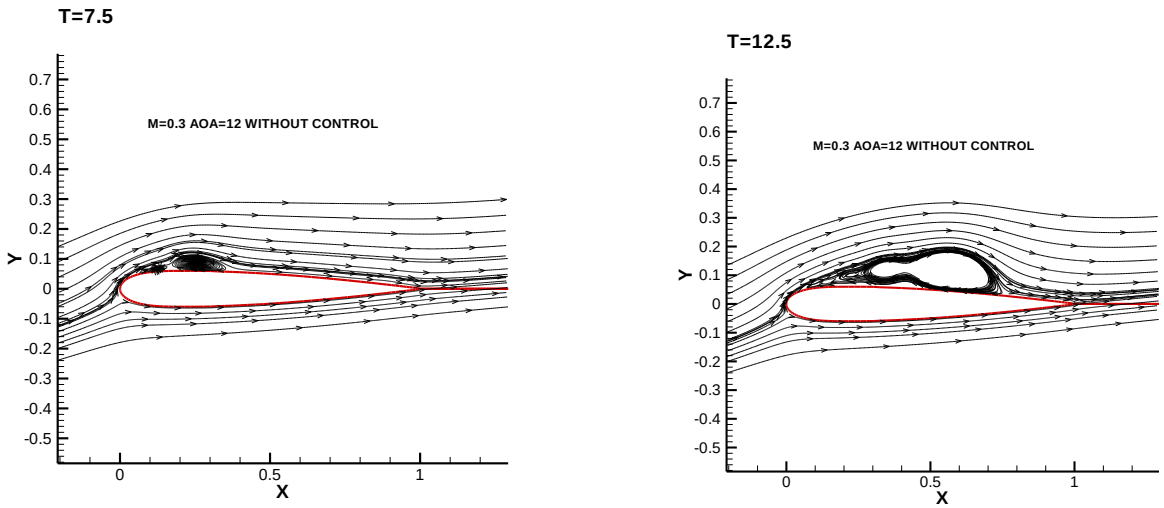

Figure 4.7 M=0.3, AOA=12, Without Control Streamlines at Different Time Instants

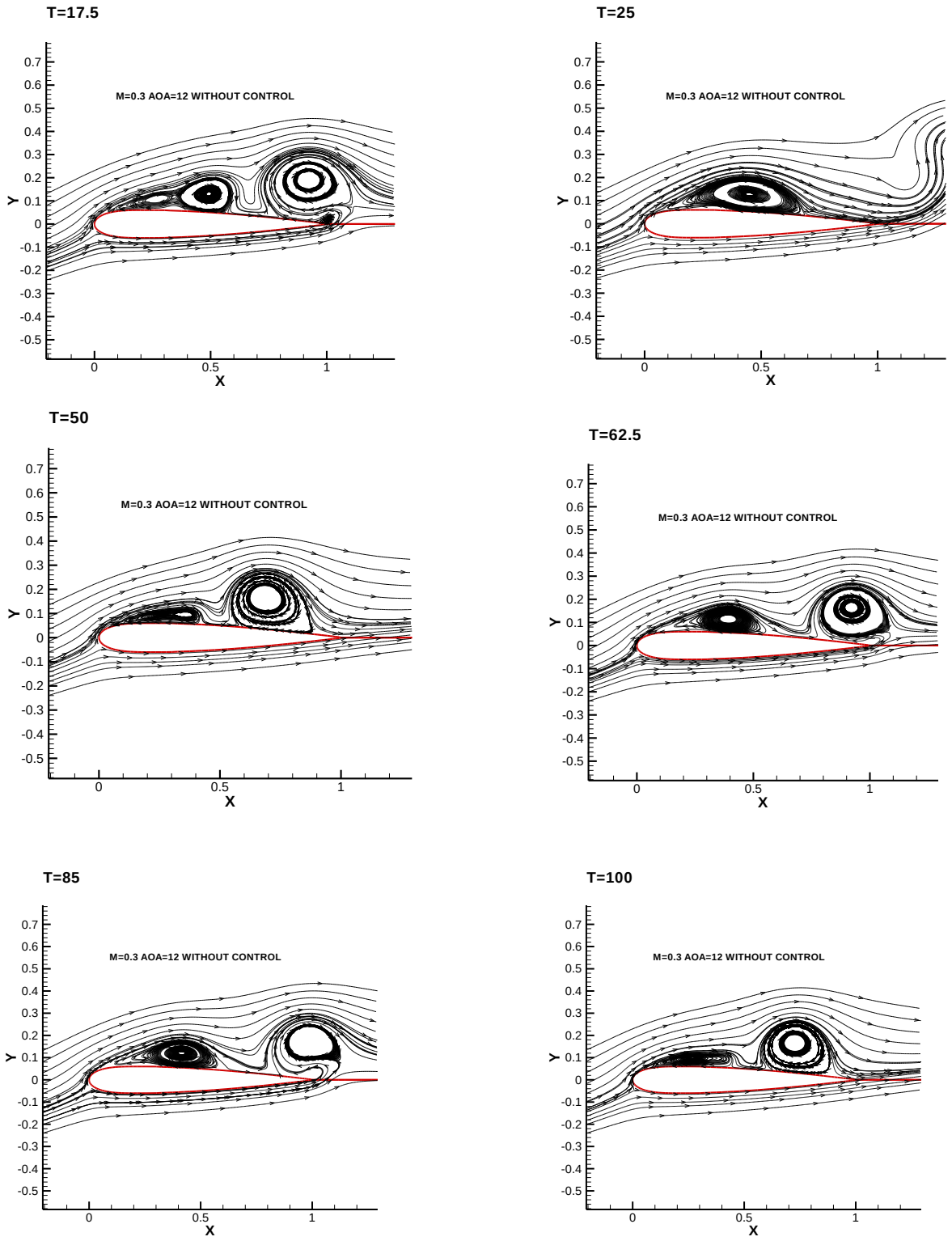

Figure 4.7 M=0.3, AOA=12, Without Control Streamlines at Different Time Instants

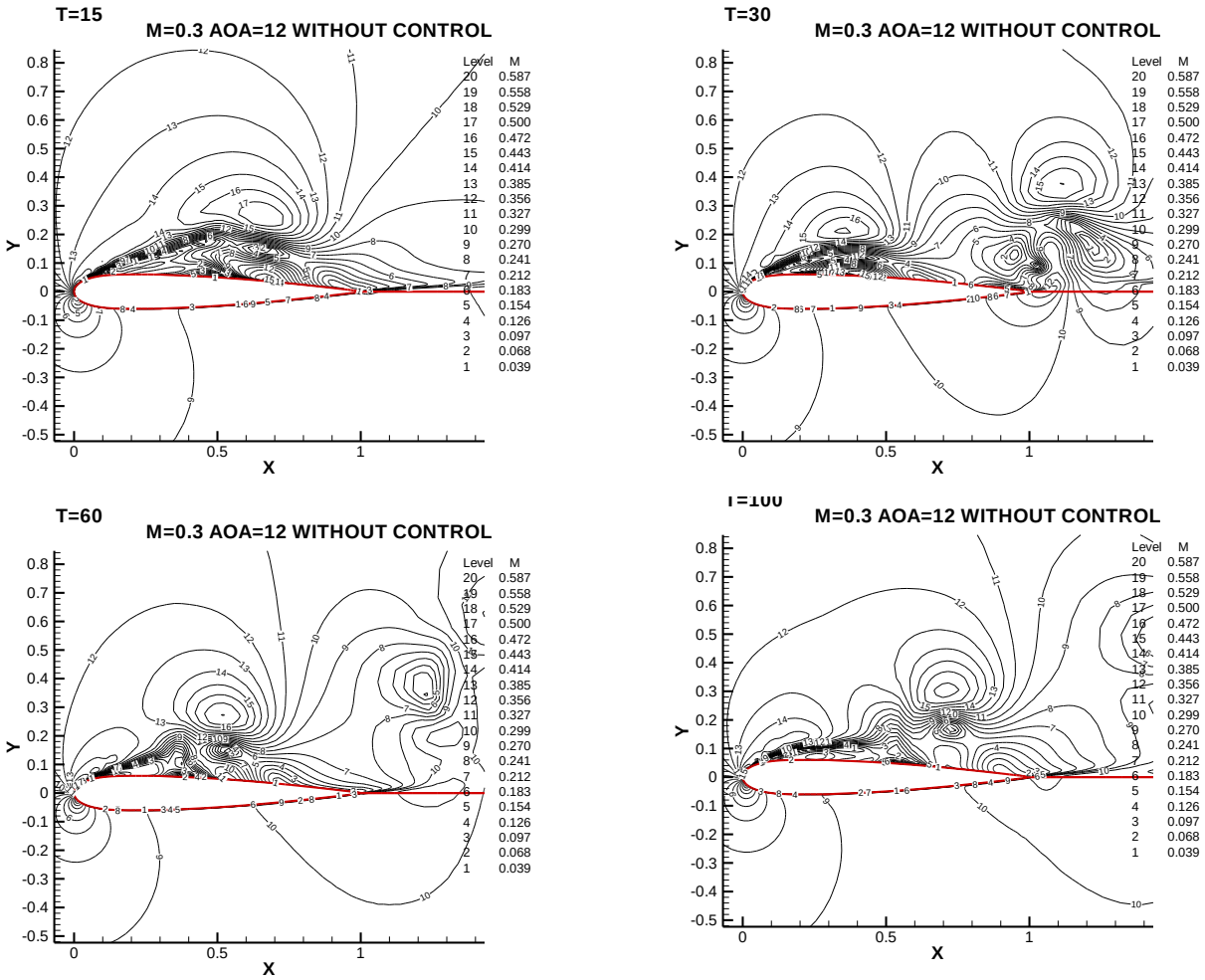

Figure 4.8 M=0.3, AOA=12, Without Control Mach Contours at Different Time Instants

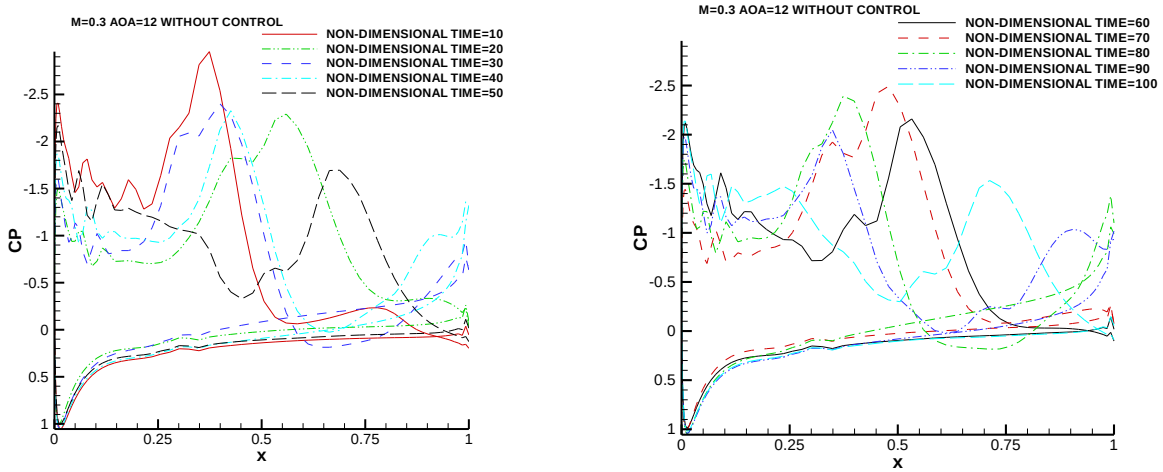

Figure 4.9 M=0.3, AOA=12, Without Control C_P Coefficient at Different Time Instants

4.2.2 Steady Suction for M=0.3 at 12 Degree of Angle Of Attack

In this calculation an array containing suction area is placed on upper surface of NACA-0012 airfoil. One steady suction area is placed at 0.08-0.14 X/C. Suction amplitude is Cq=0.13 (Mass Flow Rate). Figure 4.10 shows the suction location on airfoil. Suction is applied to surface with 70 degree of angle respect to surface normal.

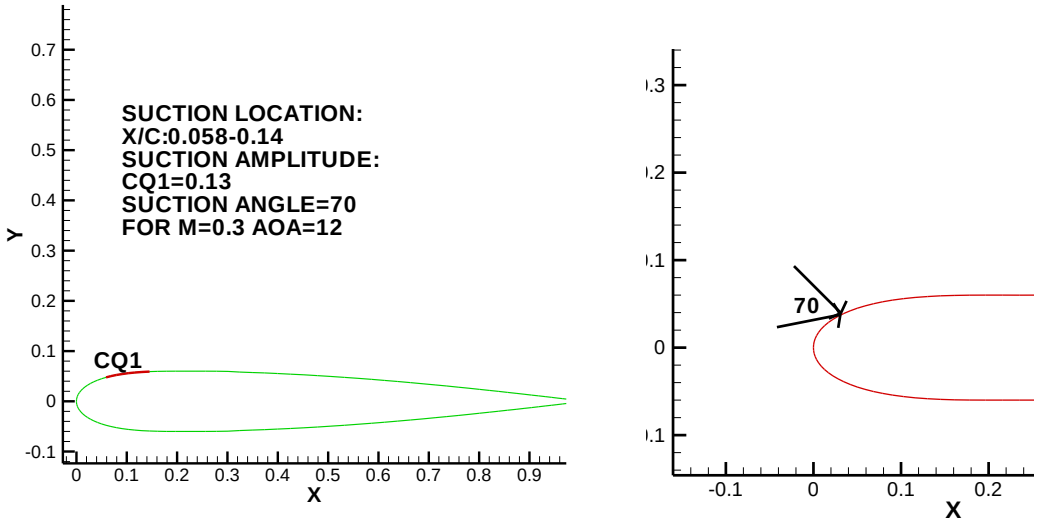

Figure4.10 Suction Location and suction angle: Steady Suction for M=0.3 at 12 Degree of Angle of Attack

Δt was obtained as $5x10^{-3}$, and fixed for all the following computations. The computations were extended to 20000 number of time step which is equivalent to non-dimensional time of T=100.

Figure shows the time history of the lift and drag coefficients comparisons with without control case. After applying steady suction oscillation amplitude become smaller. Compared with Mach number 0.3 angle of attack 12 without control case, C_L is about %25 higher and C_d is %60 lower. Table shows the comparisons between without control case and steady suction case.

Table 4.2 Lift and Drag Comparisons Between Without Control Case and Steady Suction Case

Mach number	Angle of attack	Control type	Number of suction area	Maximum C_L	Minimum C_L	Maximum C_D	Minimum C_D
0.3	12	No-control	-	1.13	0.63	0.25	0.13
0.3	12	Steady control	1	1.45	0.98	0.12	0.018

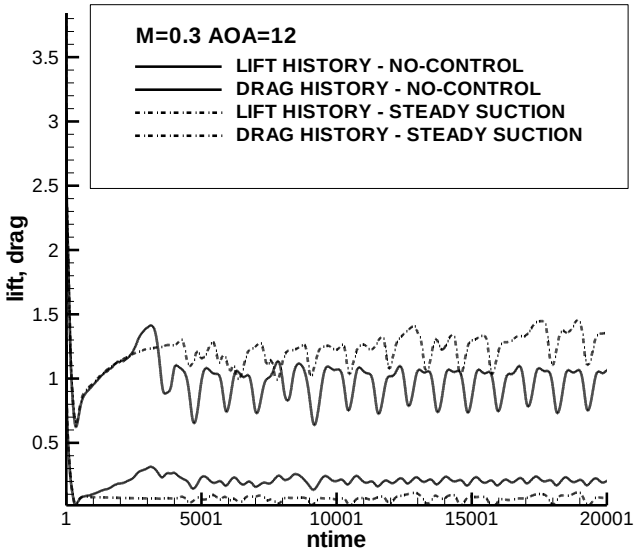

Figure 4.11 Time History of Lift and Drag Coefficient for steady control and, Without Control, M=0.3, AOA=12

Figure4.11 shows the eight snapshot views of the streamlines at several time instants. Separation starting point moved forward. The unsteady separation is development is starting from x/c 0.3. As the time goes separation develops to the trailing edge. Separation is nearly controlled compared with without control case. But there is still separation on the airfoil but it moved forward.

Figure4.12 shows the Mach Contours at different time instants. Separation location change and separation development from x/c 0.3 can be seen from the figures.

Figure4.13 shows the C_p coefficient at several different time instants. C_P coefficient shows that separation location is moved and separation is starting from x/c 0.3. And also separation amplitude became smaller compared to without control case. In this study

good results obtained but there is still separation. This result is used to control separation at next step.

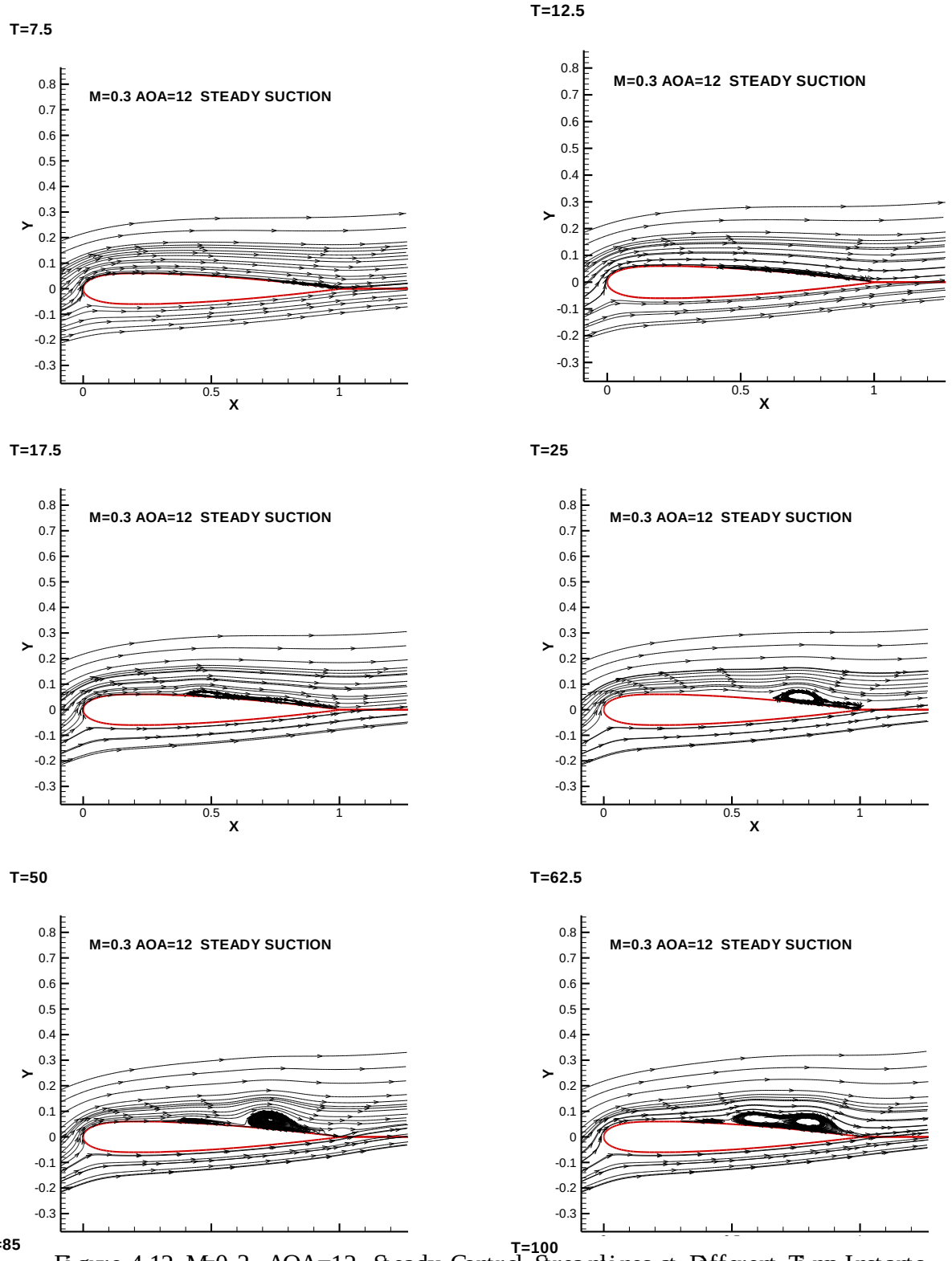

Figure 4.12 M=0.3, AOA=12, Steady Control Streamlines at Different Time Instants

Figure 4.12 M=0.3, AOA=12, Steady Control Streamlines at Different Time Instants,

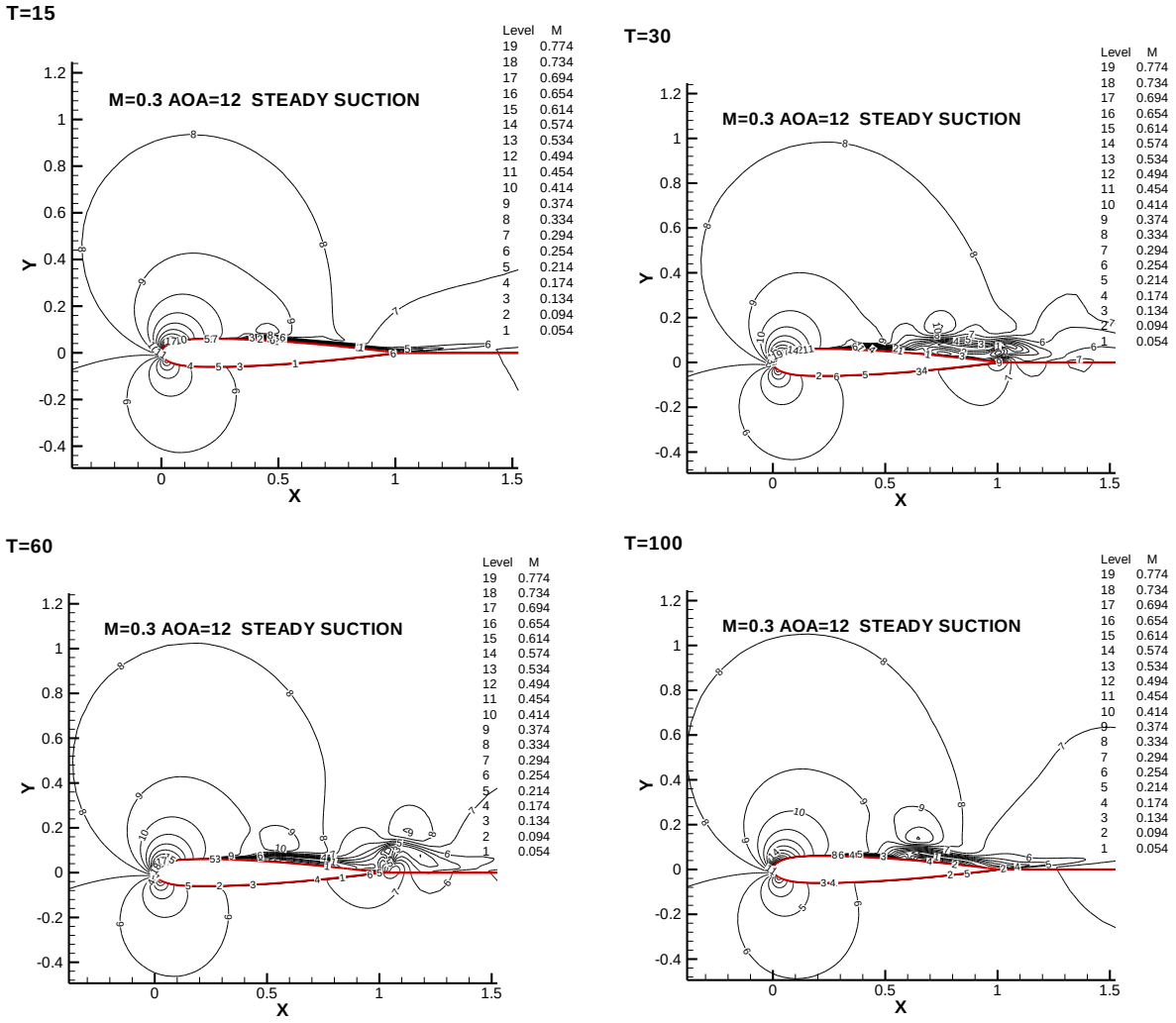

Figure4.13 M=0.3, AOA=12, steady Control, Mach Contours at Different Time Instants

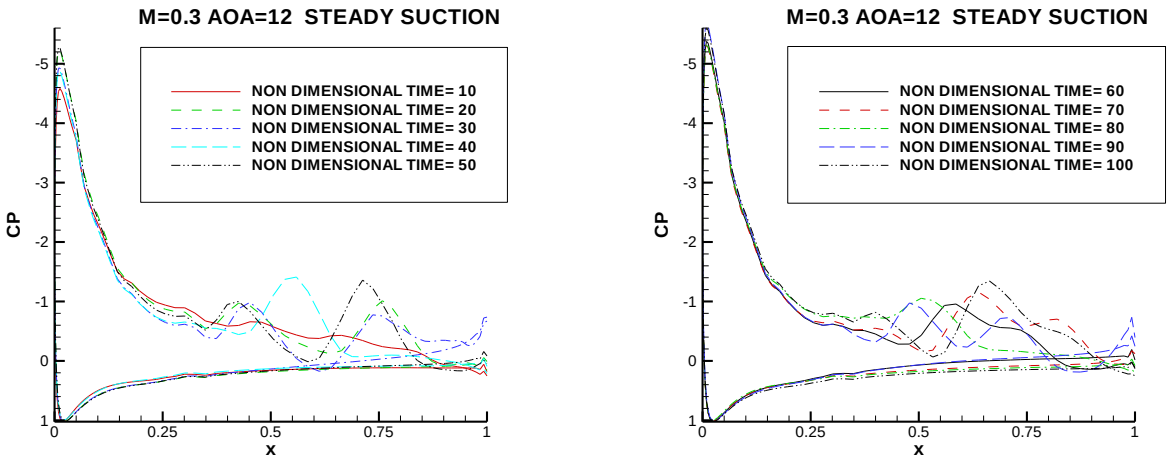

Figure 4.14 M=0.3, AOA=12, Steady Control C_P Coefficient at Different Time Instants

4.2.3 Unsteady Suction for M=0.3 At 12 Degree Of Angle Of Attack

In these calculation two arrays containing suction area is placed on upper surface of NACA-0012 airfoil. Two unsteady suction areas are placed at 0.6-0.14 X/C, and 047-0.63 X/C. Suction is applied with a frequency. Suction frequency is obtained from lift coefficient of without control case. 40 lift coefficients at different time instants were chosen and solved them by Fast Fourier Series. Suction amplitude is Cq1=-0.10-0.03*cos(1.256*time+∏/2) and cq2=-0.26-0.06*(1.256*t+∏/2) (cq=Mass Flow Rate). Steady suction cannot control separation. Cp coefficient of one steady suction case shows that separation starting development near x/c 0.45. Because of this result second suction location is applied between 047-0.63 X/C. Figure shows the suction locations on airfoil. Suction is applied to surface with 70 degree of angle respect to surface normal.

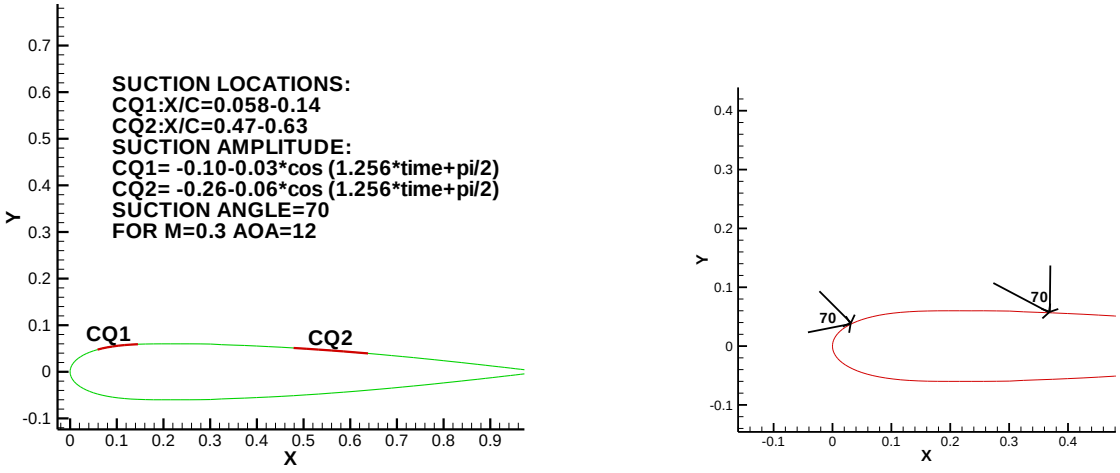

Figure4.15 Suction Location and suction angle: unsteady Suction for M=0.3 at 12 Degree of Angle of Attack

Δt was obtained as $5x10^{-3}$, and fixed for all the following computations. The computations were extended to 20000 number of time step which is equivalent to non-dimensional time of T=100.

Figure 4.15 shows the time history of the lift and drag coefficients for unsteady suction. Compared with without control case and steady suction case oscillations at drag and lift

became smaller. After applying two-unsteady suction oscillation amplitude becomes smaller. Compared with without control case and steady suction case, there is a significant increase at lift. Table4.3 shows the lift and drag comparisons between without control case, steady suction case, and unsteady suction case. Applying two unsteady suction locations does not have positive effect on drag coefficient compared with steady case.

Table 4.3 Lift and drag comparisons between no-control case, steady case and unsteady case.

Mach number	Angle of attack	Control type	Number of suction area	Maximum C_L	Minimum C_L	Maximum C_D	Minimum C_D
0.3	12	No-control	-	1.13	0.63	0.25	0.13
0.3	12	Steady control	1	1.45	0.98	0.12	0.006
0.3	12	Unsteady control	2	1.51	1.29	0.091	0.037

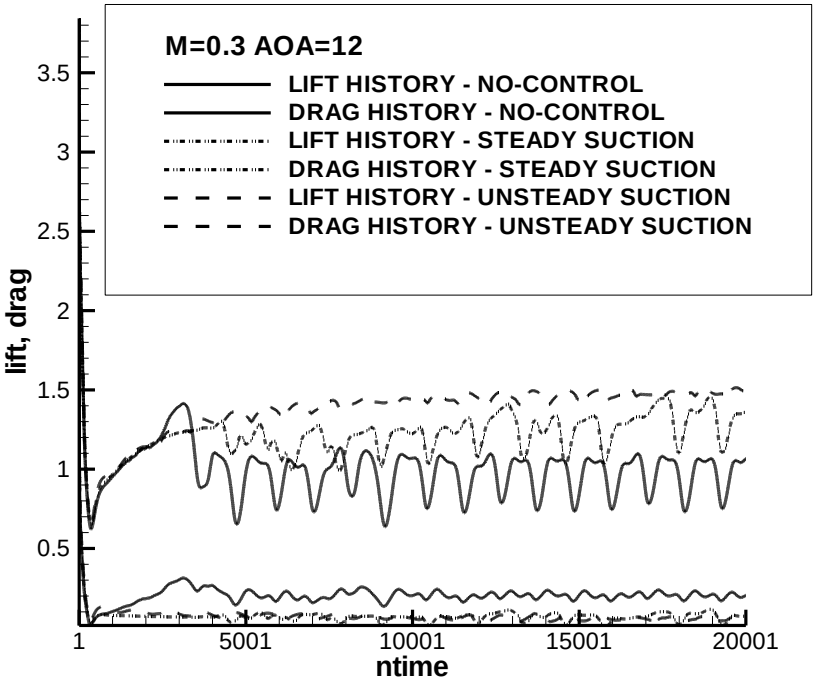

Figure4.16 Time History of Lift and Drag Coefficient, M=0.3, AOA=12, Without Control, Steady, Unsteady Control

Figure 4.16 shows the four snapshot views of the streamlines at several time instants. Separation is nearly controlled. There are small babbles on trailing edge. Figure 4.19 shows the C_p coefficient at several different time instants. These figures also prove that

T=12.5 T=12.5

separation is controlled and there are just small negative pressure gradients at trailing edge. Figure 4.18 shows the Mach Contours at different time instants. Except trailing edge Mach Contours are similar with an airfoil at zero angle of attack.

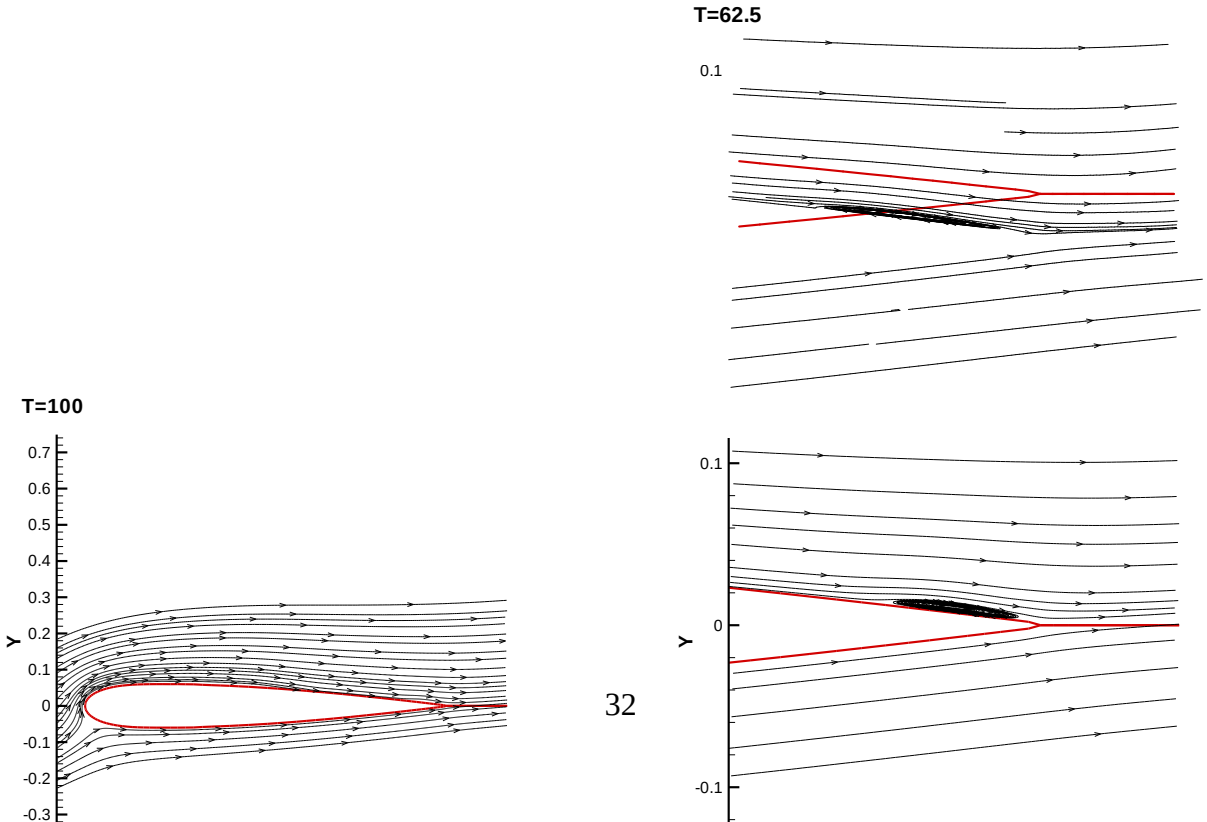

Figure 4.17 M=0.3, AOA=12, Unsteady Control Streamlines at Different Time Instants

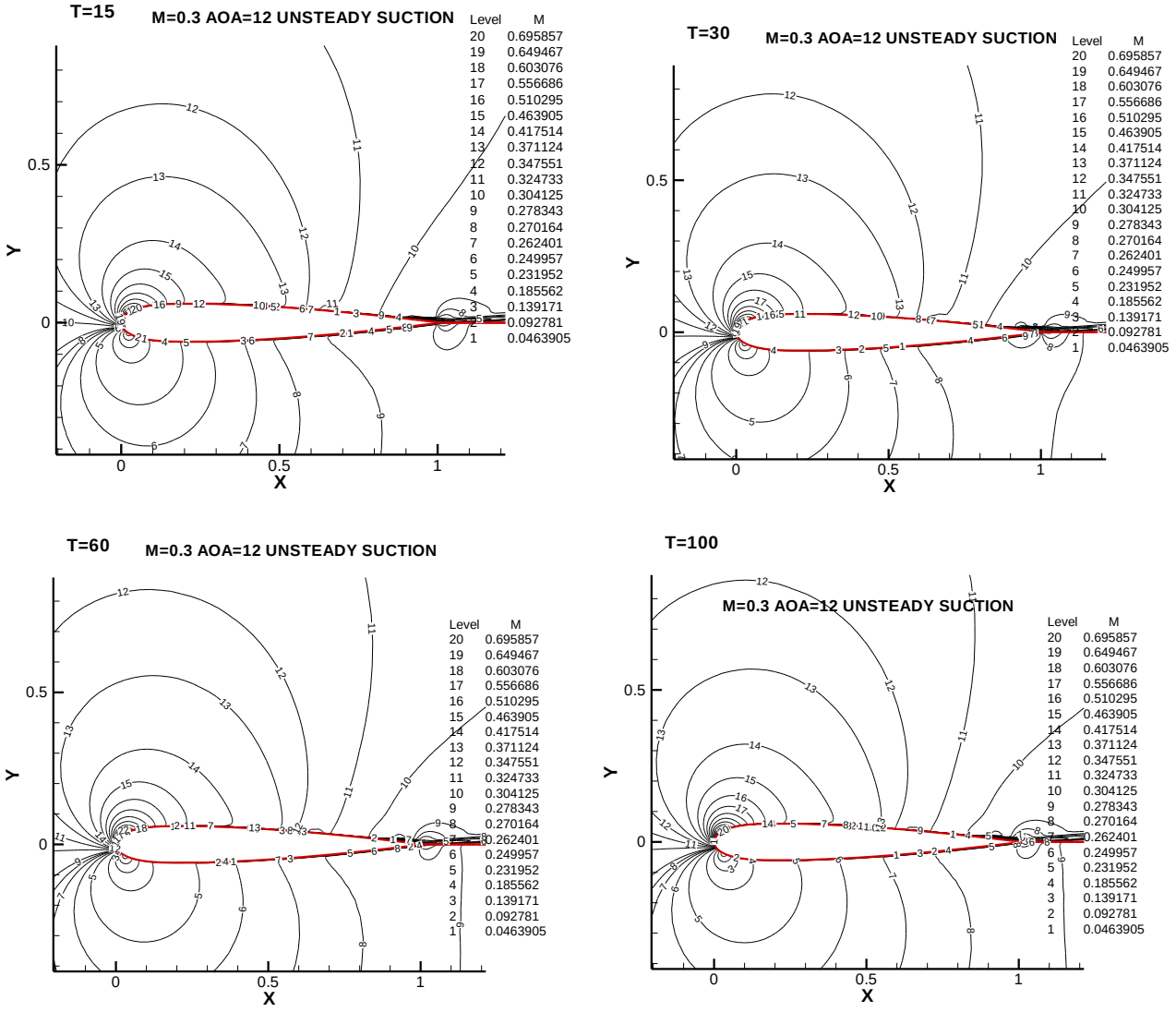

Figure4.18 M=0.3, AOA=12 Unsteady Control Streamlines at Different Time Instants

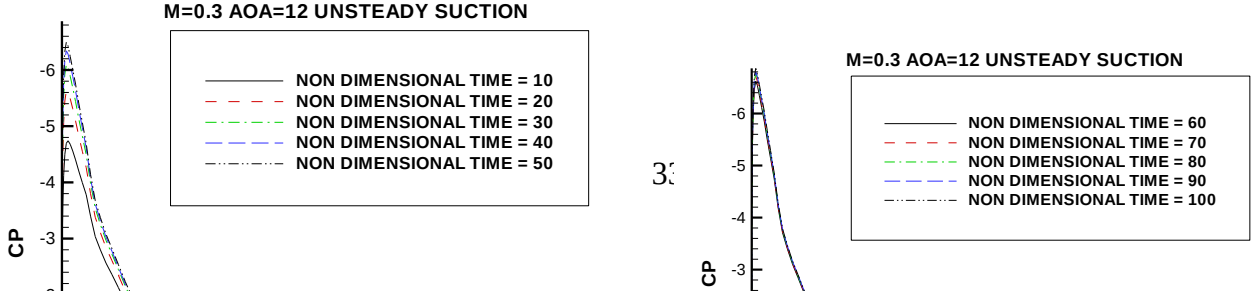

4.3 CALCULATIONS FOR 15 DEGREE OF ANGLE OF ATTACK

4.3.1 Flow Predictions for Mach number 0.3 at 15 Degree of Angle Of Attack

In same way with angle of attack 12-degree case, flow predictions for Mach number 0.3 at 15 degree of angle of attack done. Δt was obtained as $5x10^{-3}$, and fixed for all the following computations. The computations were extended to 20000 number of time step which is equivalent to non-dimensional time of T=100.

Figure 4.20 shows the time history of the lift and drag coefficient. The figure 4.20 shows oscillations at the lift and drag coefficient.

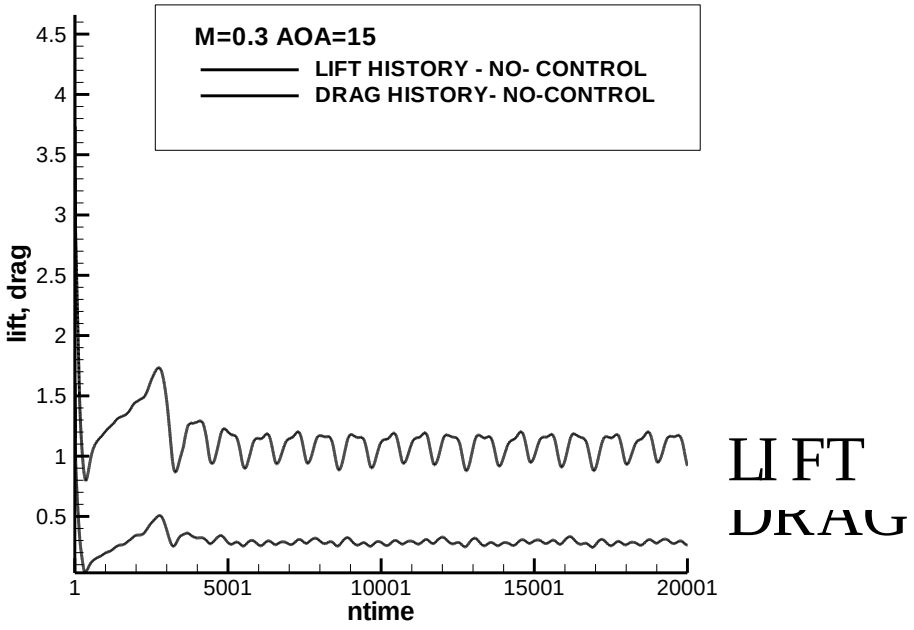

Figure4.20 Time History of Lift and Drag Coefficient, M=0.3, AOA=12, Without Control

Except for transient time (0-4000 number of time step), the lift coefficient shows larger amplitude oscillations than drag coefficient.

The maximum lift coefficient is 1.22 and the minimum lift coefficient is 0.87. The maximum drag coefficient is 0.34 and the minimum drag coefficient is 0.24. Oscillations at the lift and drag coefficient is unsteady and it is not possible to obtain an exact frequency. The continuous oscillations of the lift and drag coefficient is mainly due to the unsteady separation.

Figure 4.21 shows the eight-dimensional snapshot views of the streamlines at several time instants. The unsteady separation development is clearly observed. Separation development is more severe than angle of attack 12 case. As the time goes separation starts near the leading edge and develops into a strong unsteady separated flow. Figure shows 4.23 the Mach contours at different time instants. The development of unsteady separation can be seen. Figure 4.22 shows the C_p coefficient at several different time instants. C_P coefficient shows that separation is unsteady. The peak point of CP coefficient shows the separation location. Separation location differs in time.

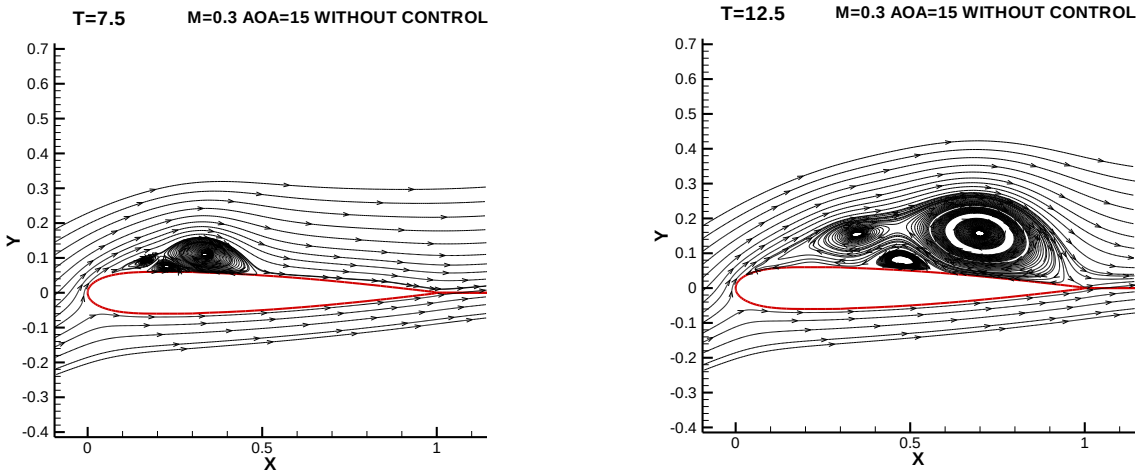

Figure4. 21 M=0.3, AOA=15, Without Control, Streamlines At Different Time Instants

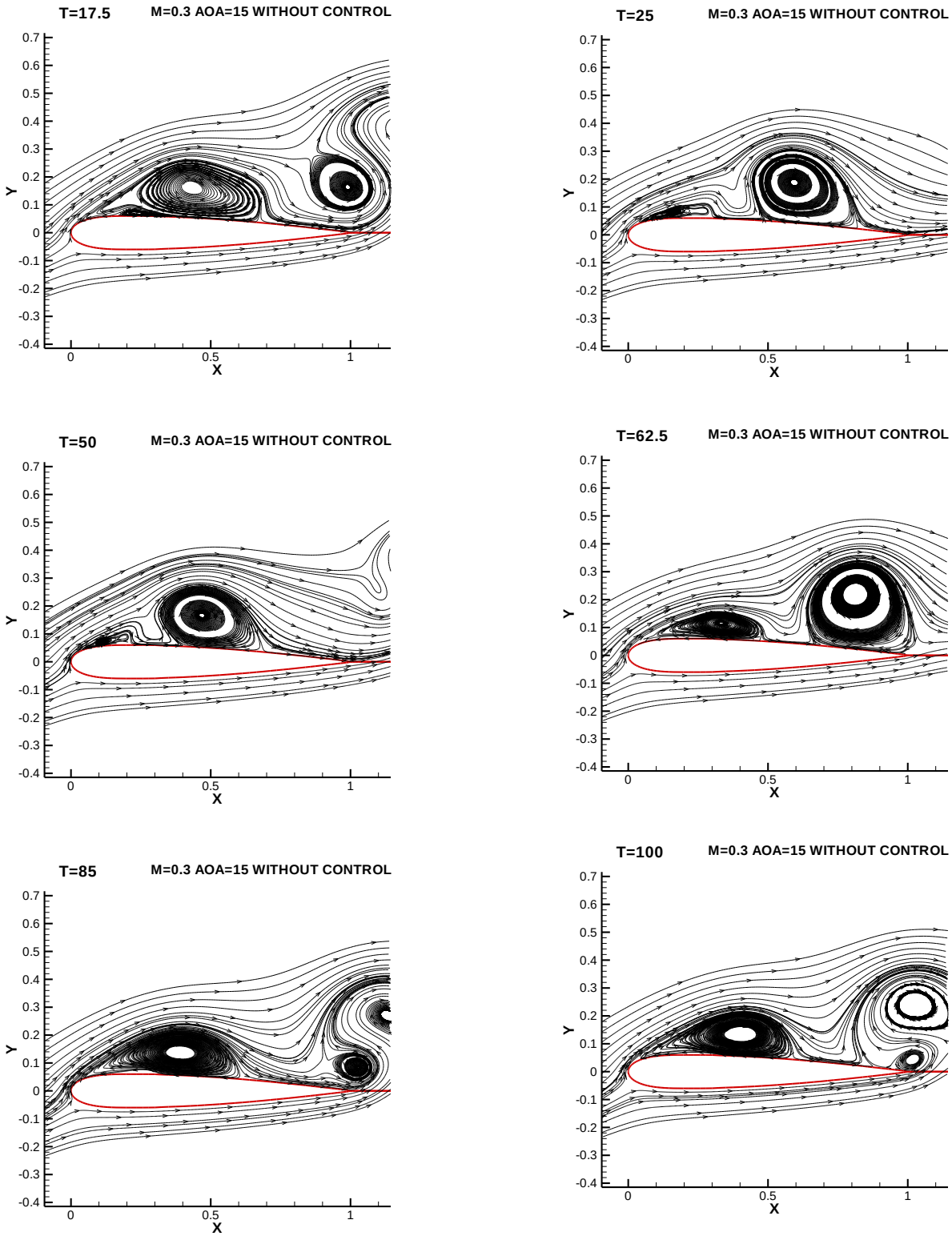

Figure4. 21 M=0.3, AOA=15, Without Control, Streamlines At Different Time Instants

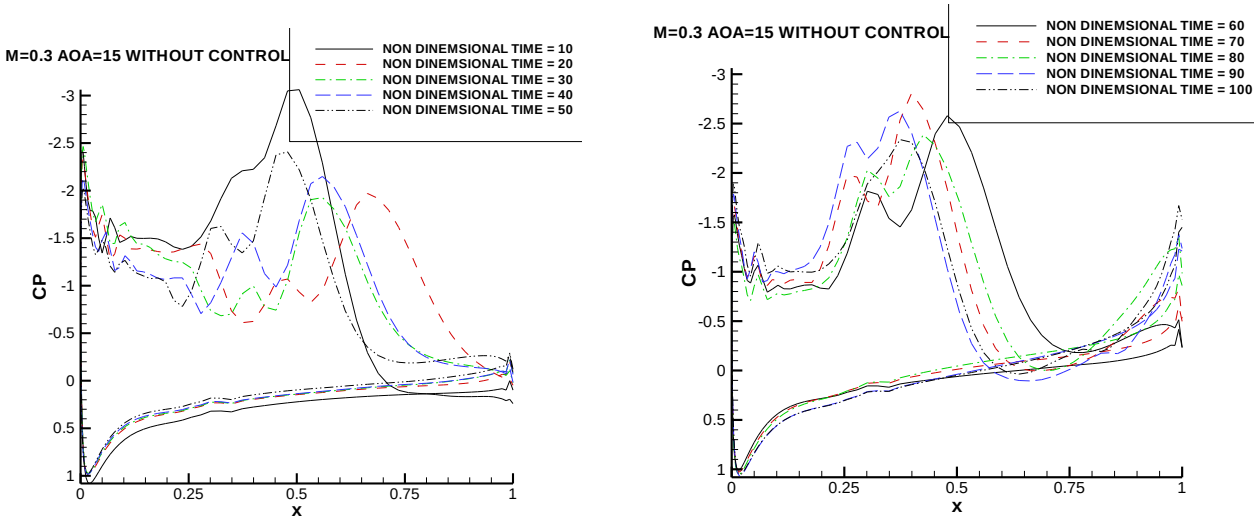

Figure4.23 M=0.3, AOA=12, Without Control, C_p Coefficient at Different Time Instants

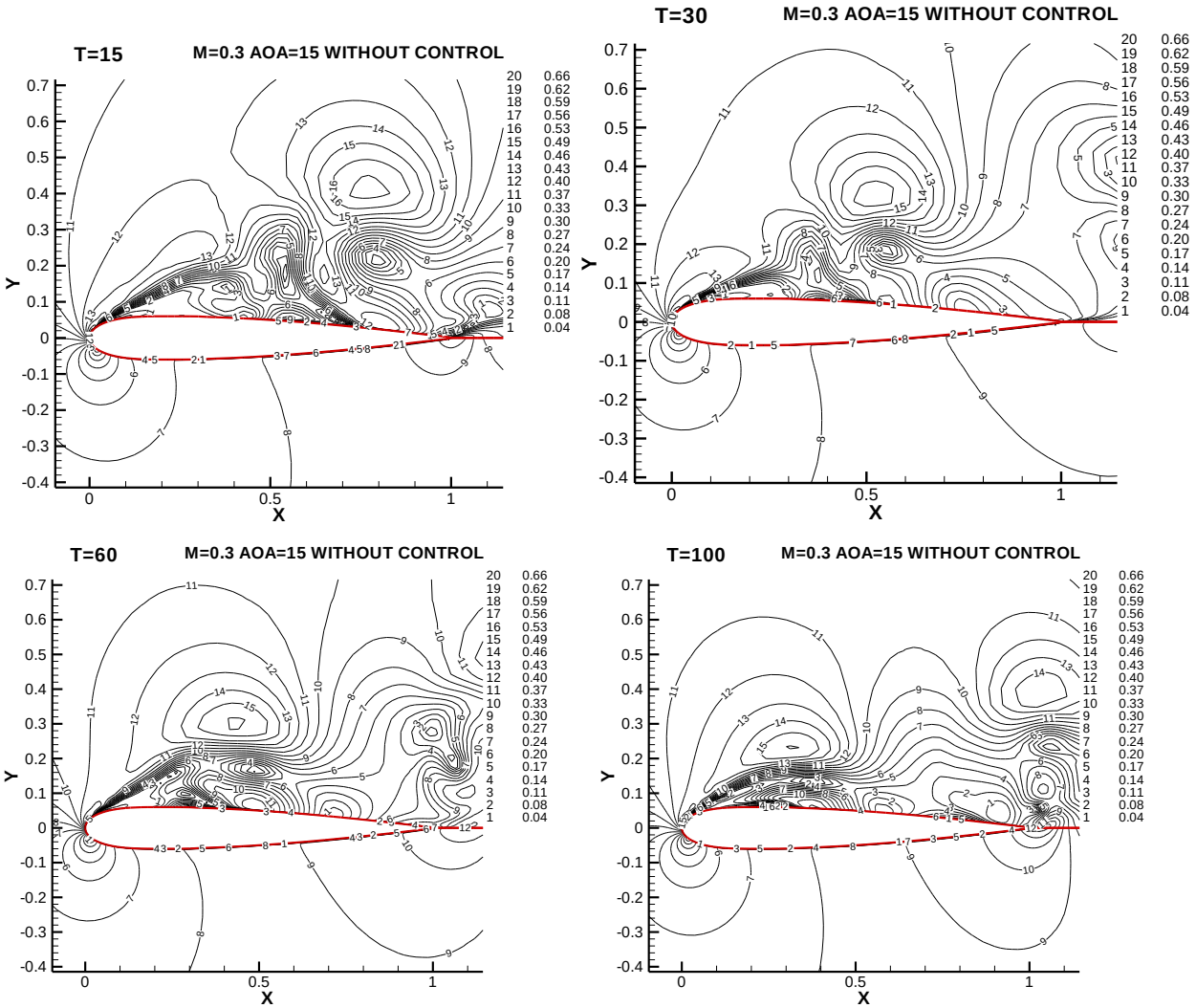

Figure4.22 M=0.3, AOA=15, Without Control, Mach Contours at Different Time Instants

4.3.2 Steady Suction for M=0.3 at 15 Degree of Angle Of Attack

In this calculation an array containing suction area is placed on upper surface of NACA-0012 airfoil. One steady suction area is placed at $0.050 \le x/c \le 0.14$. Suction amplitude is Cq=0.13 (Mass Flow Flux). Figure 4.24 shows the suction location on airfoil. Suction is applied to surface with 70 degree of angle respect to surface normal.

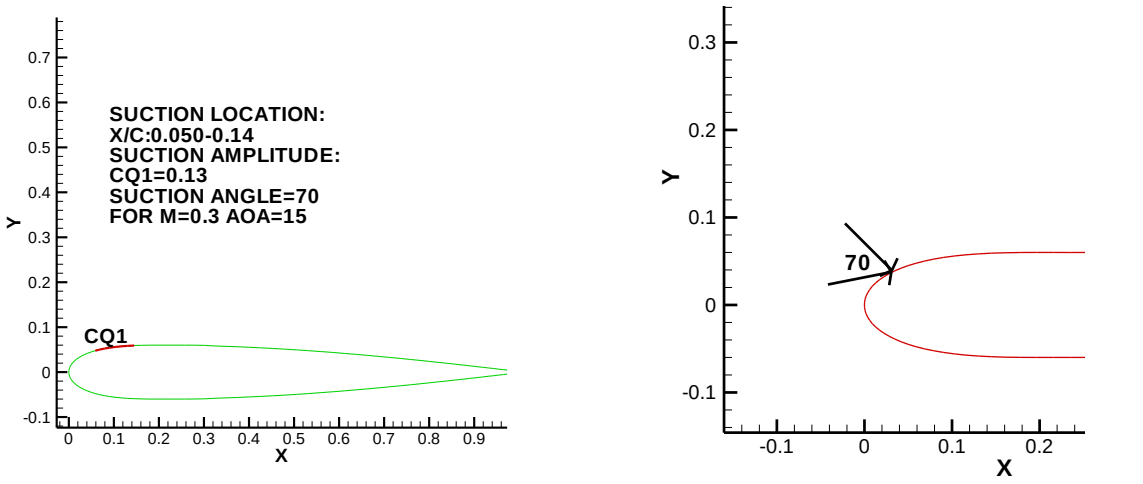

Figure4.24 Suction Location and suction angle: Steady Suction for M=0.3 at 15 Degree of Angle of Attack

Δt was chosen as $5x10^{-3}$, and fixed for all the following computations. The computations were extended to 20000 number of time step which is equivalent to non-dimensional time of T=100.

Figure 4.25 shows the time history of the lift and drag coefficients comparisons with without control case for angle of attack 15. After applying steady suction oscillation amplitude become smaller. Compared with Mach number 0.3 angle of attack 15 without control case, C_L is about %12-18 higher and C_d is %67 lower. Table 4.4 shows the comparisons between without control case and steady suction case.

Table 4.4 lift and drag comparisons between without control and steady suction case

Mach number	Angle of attack	Control type	Number of suction area	Maximum C_L	Minimum C_L	Maximum C_D	Minimum C_D
0.3	15	No-control	-	1.22	0.87	0.34	0.24
0.3	15	Steady control	1	1.45	0.98	0.11	0.04

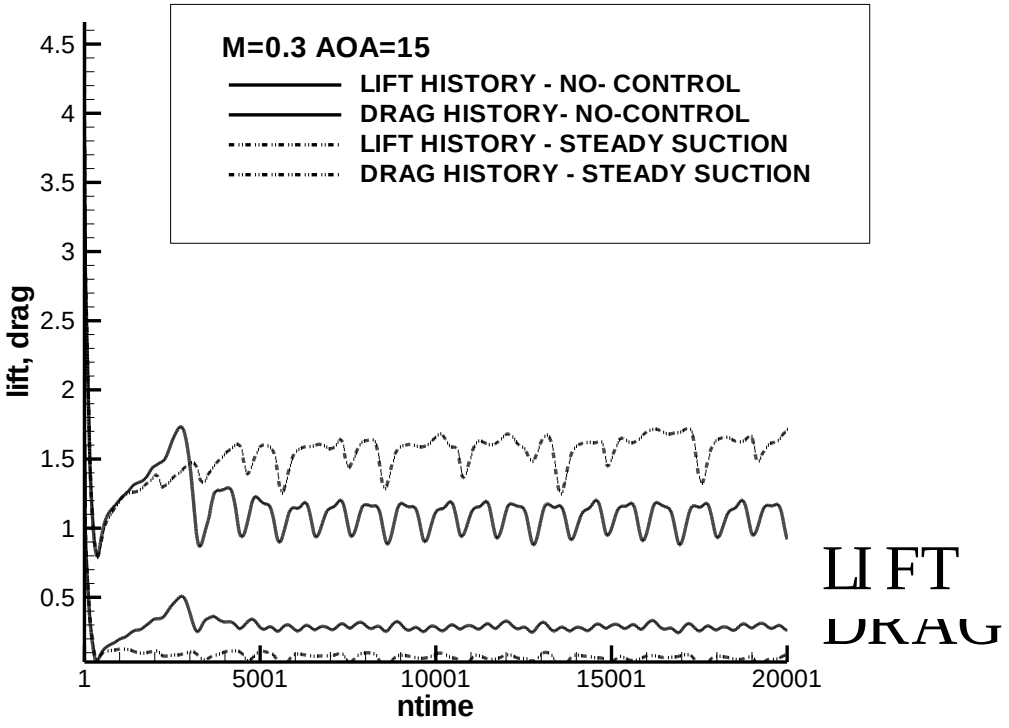

Figure 4.25 Time History of Lift and Drag Coefficient, M=0.3, AOA=15, Without Control and Steady Control

Figure 4.26 shows the eight snapshot views of the streamlines at several time instants. Separation starting point moved forward. The unsteady separation development is starting from x/c 0.3. As the time goes separation develops to the trailing edge. Separation is nearly controlled compared with without control case. But there is still separation on the airfoil but it moved forward.

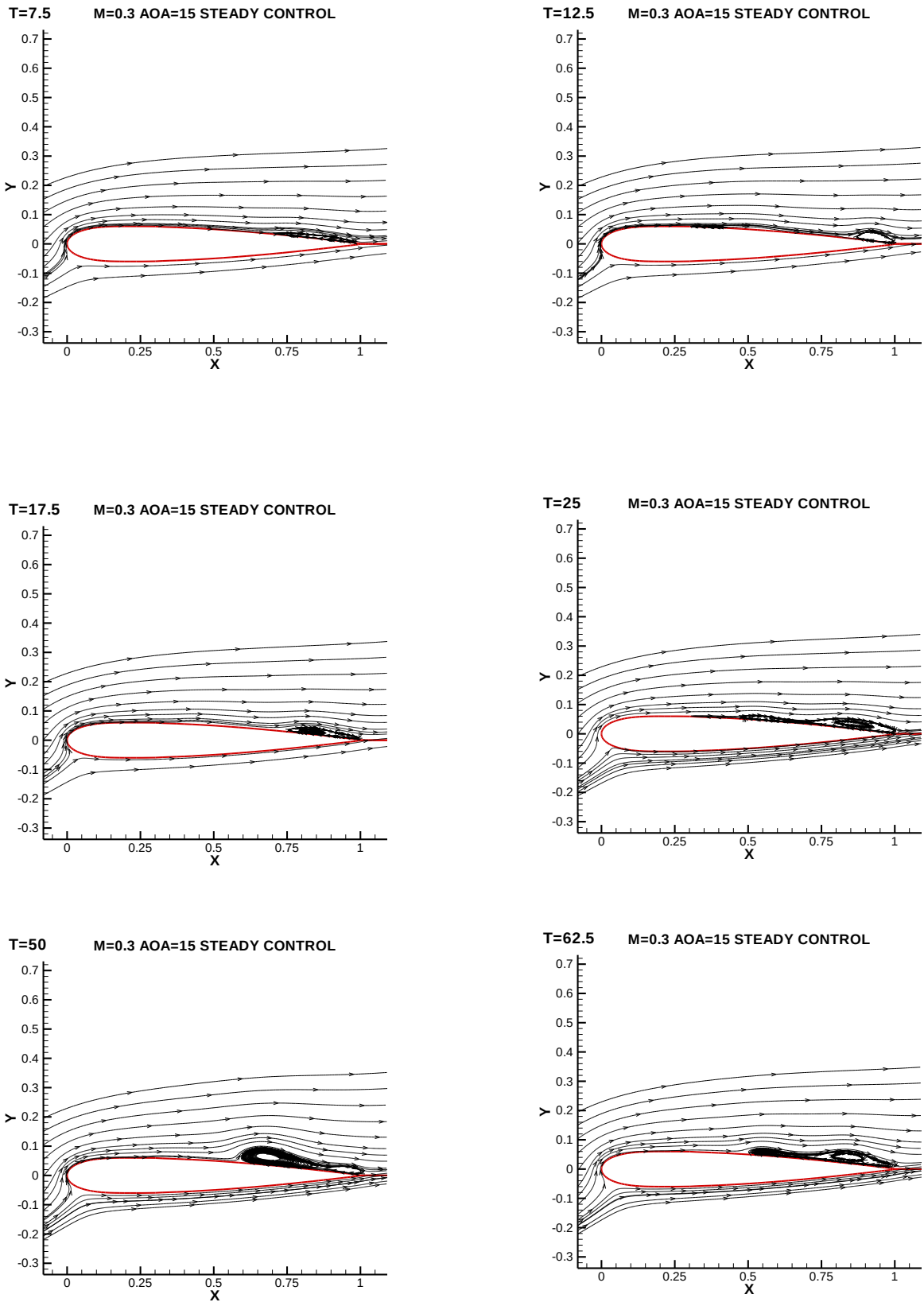

Figure 4.26 M=0.3, AOA=15, Steady Control Streamlines at Different Time Instants

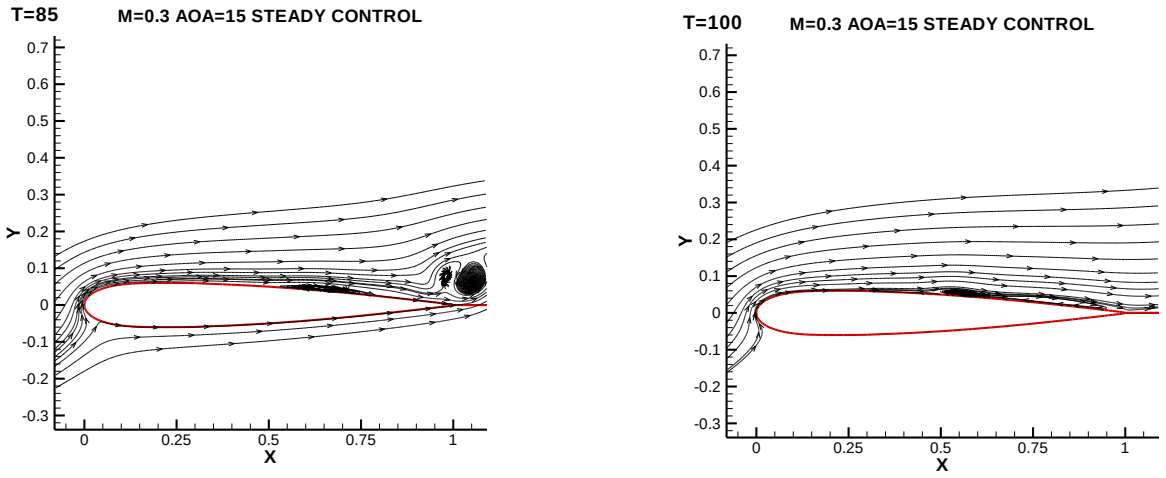

Figure 4.26 M=0.3, AOA=15, Steady Control Streamlines at Different Time Instants

Figure 4.28 shows the Mach Contours at different time instants. Separation location change and separation development from x/c 0.3 can be seen from the figures.

Figure 4.27 shows the C_p coefficient at several different time instants. C_P coefficient shows that separation location is moved and separation is starting from x/c 0.3. And also separation amplitude became smaller compared to without control case. In this study good results were obtained but there is still separation. This case's result is used to control separation at next step.

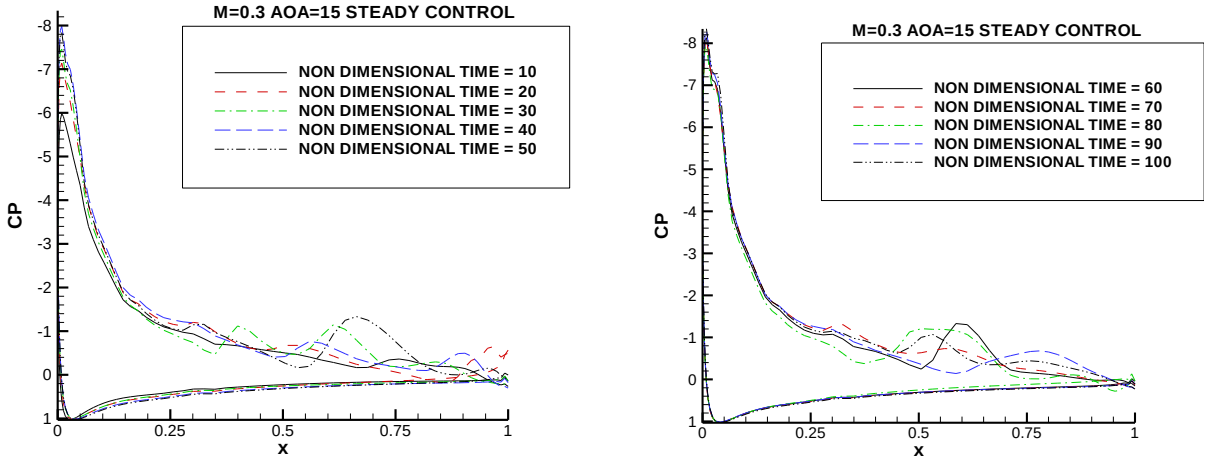

Figure 4.27 M=0.3, AOA=15, Steady Control C_p Coefficient at Different Time Instants

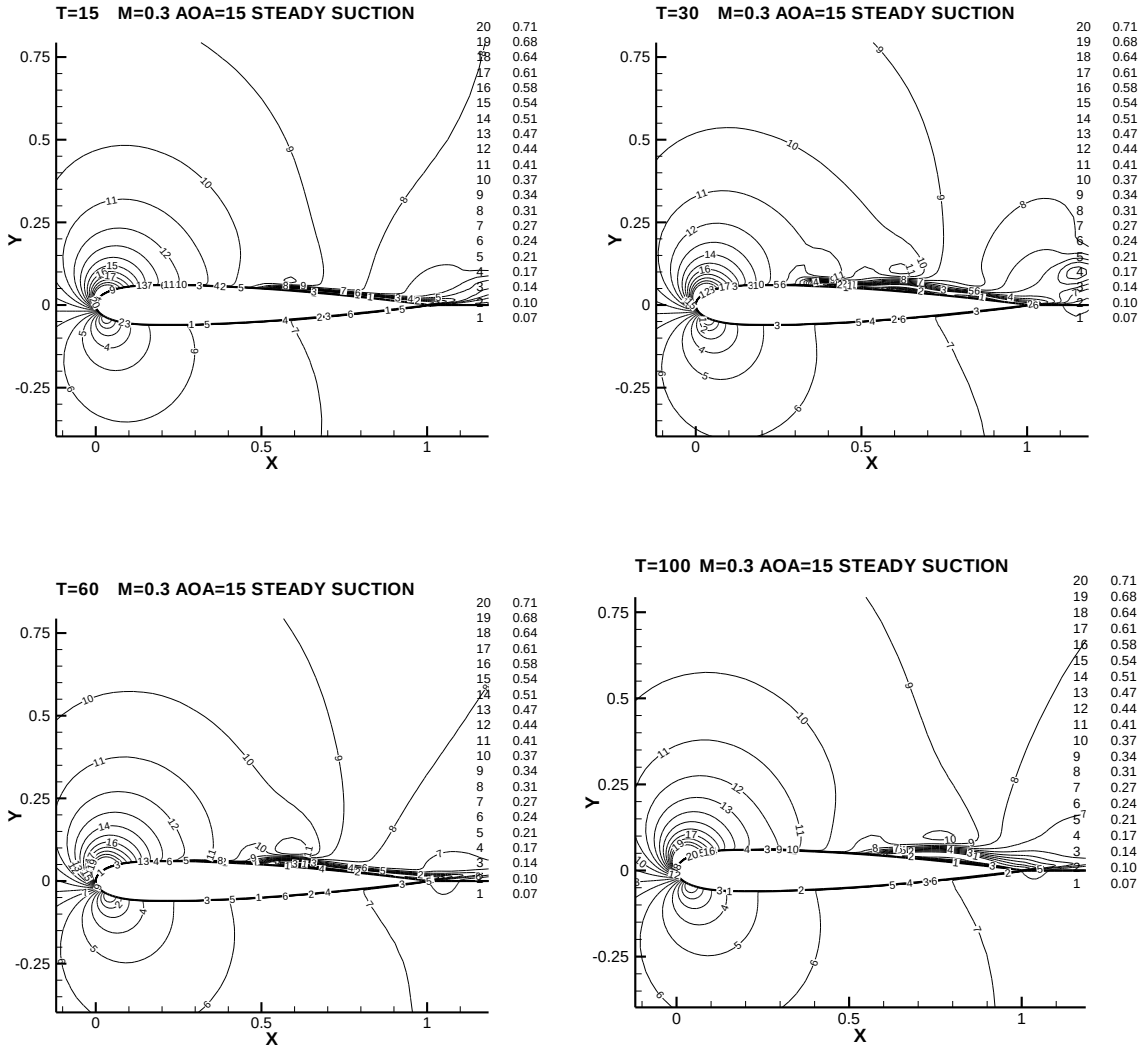

Figure 4.28 M=0.3, AOA=15, Steady Control Mach Contours at Different Time Instants

4.3.3 Unsteady Suction for M=0.3 at 12 Degree Angle Of Attack

In these calculation two arrays containing suction area is placed on upper surface of NACA-0012 airfoil. Two unsteady suction areas are placed at 0.058-0.16 X/C, and 0.34-05 X/C. Suction is applied with a frequency. Suction frequency is obtained from lift coefficient of without control case. 40 lift coefficients at different time instants chosen and solved them by Fast Fourier Series. Suction amplitude is Cq1=-0.10-0.03*cos(1.256*time+∏/2) and cq2=-0.18-0.06*(1.256*t+∏/2) (cq=Mass Flow Rate). Separation is not controlled. Cp coefficient of one steady suction case shows that separation starting development near x/c 0.40. Because of this result second suction location is applied between 0.34-0.5 X/C. Figure 4.29 shows the suction locations on airfoil. Suction is applied to surface with 70 degree of angle respect to surface normal.

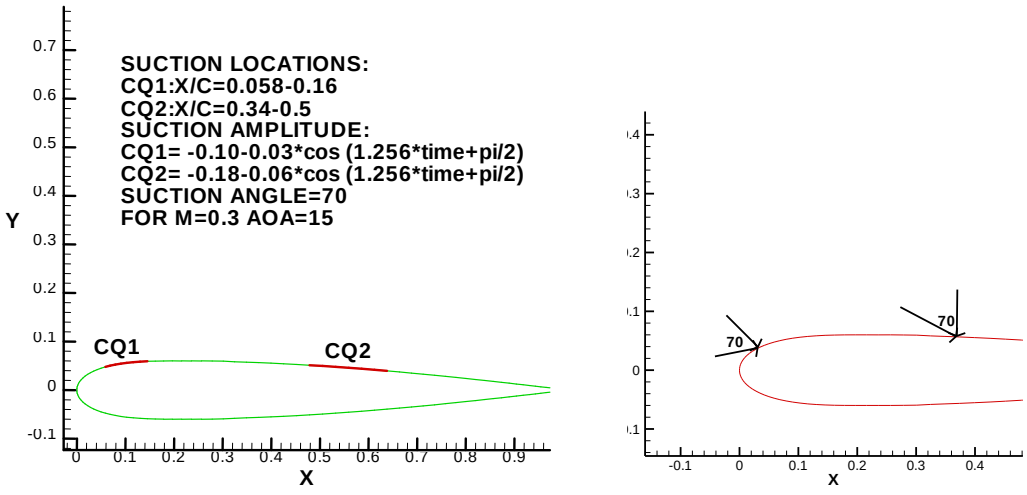

Figure4.29 Suction Location and suction angle: Steady Suction for M=0.3 at 15 Degree of Angle of Attack

Δt was obtained as $5x10^{-3}$, and fixed for all the following computations. The computations were extended to 20000 number of time step which is equivalent to non-dimensional time of T=100.

Figure 4.30 shows the time history of the lift and drag coefficients for unsteady suction. Compared with without control case and steady suction case oscillations at drag and lift

became smaller. After applying two-unsteady suction oscillation amplitude becomes smaller. Compared with without control case and steady suction case, there is a significant increase at lift. Tables 4.5 show the lift and drag comparisons between without control case, steady suction case, and unsteady suction case. Applying two unsteady suction locations does not have positive effect on drag coefficient compared with steady case.

Table 4.5 Lift and Drag Comparisons Between Without Control Case and Steady Control, Unsteady Control

Mach number	Angle of attack	Control type	Number of suction area	Maximum C_L	Minimum C_L	Maximum C_D	Minimum C_D
0.3	15	No-control	-	1.22	0.87	0.34	0.24
0.3	15	Steady control	1	1.45	0.98	0.11	0.02
0.3	15	Unsteady control	2	1.61	1.82	0.11	0.043

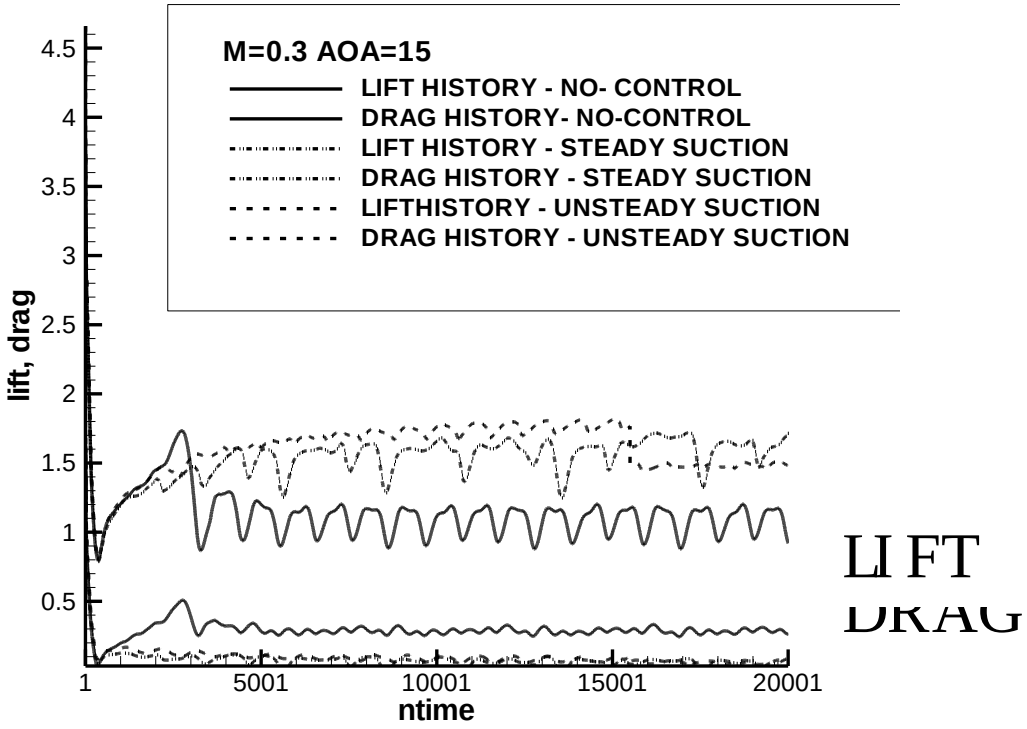

Figure 4.30 Time History of Lift and Drag Coefficient, M=0.3, AOA=15, Without Control, Steady, Unsteady Control

Figure 4.31 shows the four snapshot views of the streamlines at several time instants. Separation is nearly controlled. There are small bobbles on trailing edge. Figure4.33 shows the C_p coefficient at several different time instants. These figures also prove that separation is controlled and there are just small negative pressure gradients at trailing edge. Figure 4.32 shows the Mach Contours at different time instants. Except trailing edge Mach Contours are similar with an airfoil at zero angle of attack.

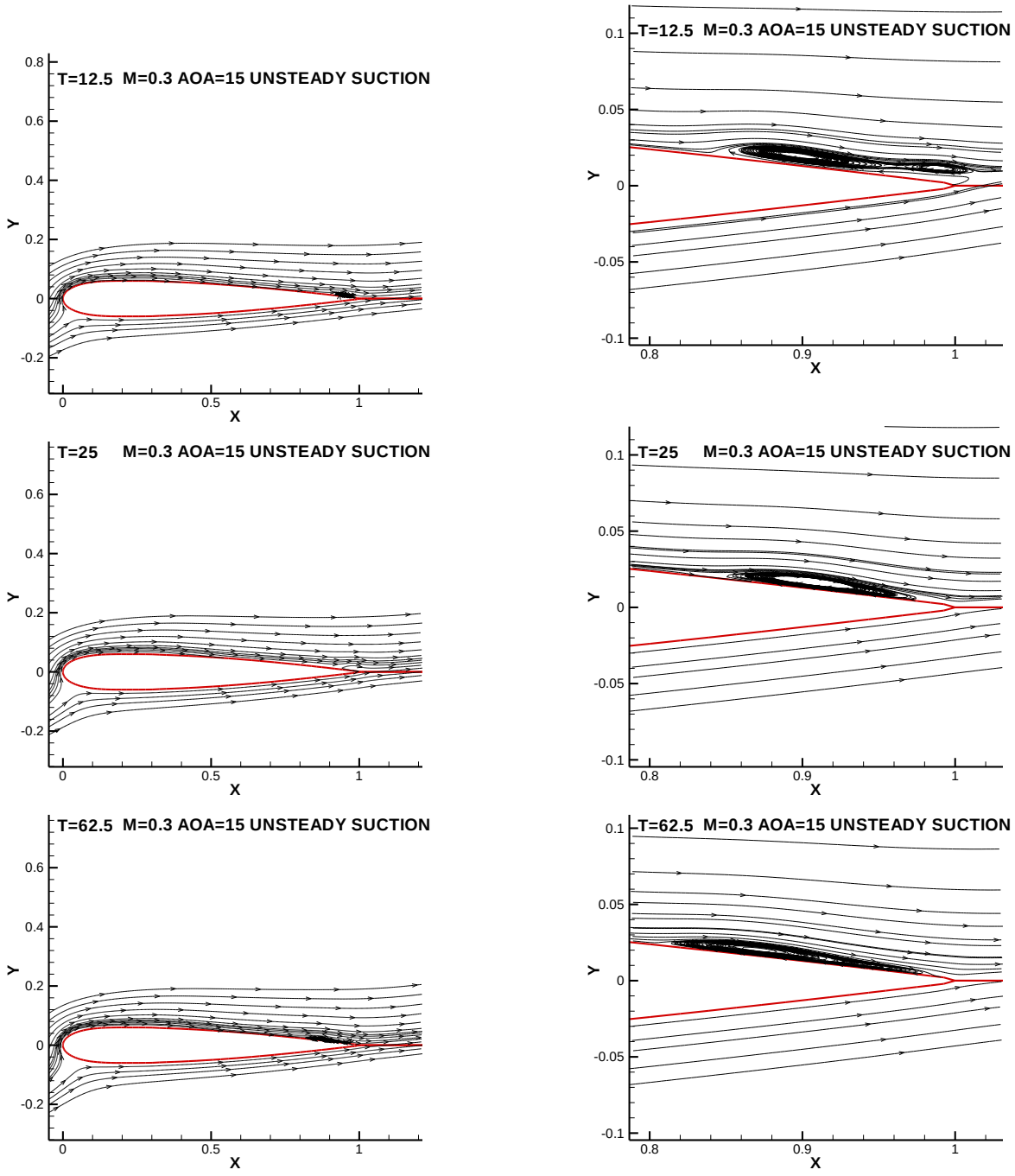

Figure 4.31 M=0.3, AOA=15, Steady Control Streamlines at Different Time Instants

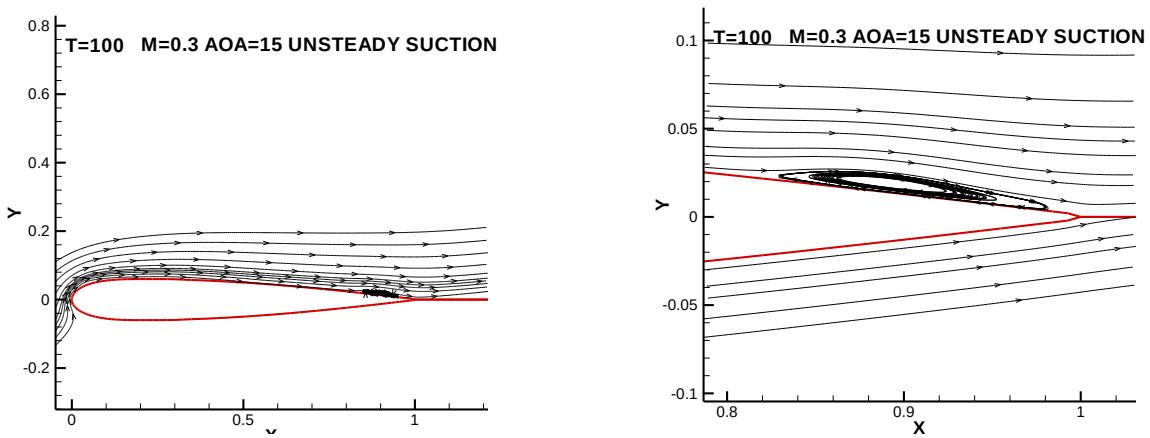

Figure 4.31 M=0.3, AOA=15, Steady Control Streamlines at Different Time Instants

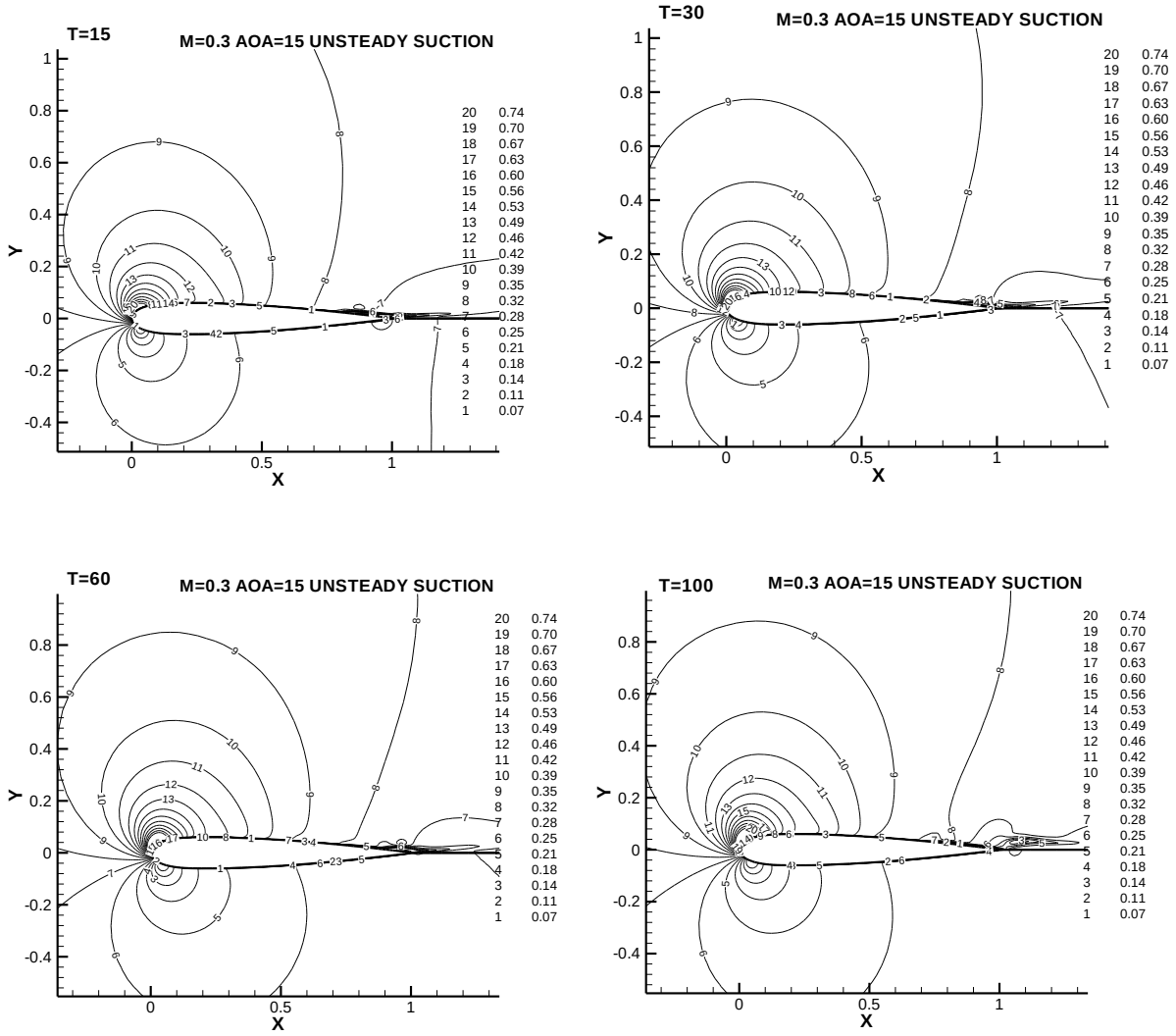

Figure 4.32 M=0.3, AOA=15, Unsteady Control Mach Contours at Different Time Instants

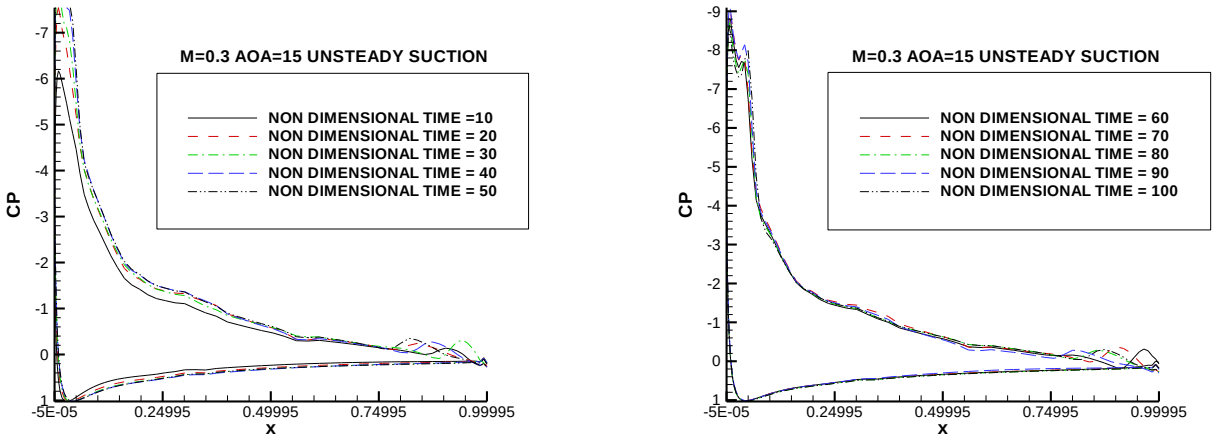

Figure 4.33 M=0.3, AOA=15, Unsteady Control C_p Coefficient at Different Time Instants

5. CONCLUSIONS AND RECOMMENDATIONS

Separation control for an airfoil is studied at different angle of attacks by using CFL3D (V5), a Reynold-Avaraged thin-layer Navier-Stokes flow solver. Steady or unsteady suction is applied on a fixed area with certain angle. At 12 and 15 degrees of angle of attack, separation is controlled. Numerical results indicated that, application of unsteady oscillatory suction with angle could control separation. Moreover, improved values are obtained for lift and drag by applying suction.

Numerical studies indicated that there is interaction between suction location, suction magnitude, suction area and suction angle. Separation location and magnitude change in time. Therefore, we will mention about suction amplitude and suction location.

5.1 Suction Location

It is not easy to obtain the exact suction location. Separation point moves and changes in time. High negative pressure gradients indicate presence of separation. From Cp coefficients, suction location can be guessed. As the angle of attack increase, separation location moves toward the leading edge. Final suction location is determined based on the results of several trial runs.

5.2 Suction Amplitude

Final suction amplitude is determined from several trial runs. A suction flow ratio of 0,13 is employed at the leading edge. For unsteady cases oscillatory suction is applied. Oscillation frequency is determined based on lift histories, through FFT of lift history.

Determination of optimum suction angle, frequency and amplitude for automatic control of separation, requires further study.

REFERENCES

[1] **Herbst, W.B**, 1985, Dynamics of Air Combat, J. Aircraft, Vol. 20, No. 7, Pp 594-598.

[2] **Herbst, W.B**, 1985, Super maneuverability Workshop on Unsteady Separated Flows, Pp1-8.

[3] **Whitford, R**, 1987, Design for Air Combat, Jane's Publishing Company Limited, New York, NY.

[4] **John A. Ekaterinaris, Max F. Platzer**, 1998, Computational Predictions Of Airfoil Dynamic Stall, Aerospace Science, Vol. 33, Pp 759-846, Elsevier Science Ltd.

[5] **Schlilting, H**. 1978, Boundary Layer Theory, seventh Edition, McGraw Hill Book Company, New York, Pp 34 and 132.

[6] **Ekaterinaris A John**, March-April 2002, Numerical Investigation Of Dynamic Stall Control Via Airfoil Thickness Variations, Journal Of Aircraft Vol., No. 2.

[7] **Gad-El-Hak**., 1990, Control of Low-Speed Airfoil Aerodynamics, AIAA Journal, Vol. 28, No. 9, Pp. 1537-1552.

[8] **Jason T. Lachowicz, Chung-Sheng Yao and Richard W. Wlezien**, Jan., 12-15, 1998 Scaling Of An Oscillatory Flow-Control Actuator, AIAA 98-0330, 36th Aerospace Sciences Meeting Exhibit, Reno, NV.

[9] **Katz, Y. Horev, E. And Wygnanski, I.**, 1992, The Forced Turbulent Wall Jet, Journal Of Fluid Mechanics, Vol. 242, Pp. 577-609.

[10] **Seifert, A. Bachar, T., Wygnanski, I., Koss, D., And Shepelovich, M.,** 1993, Oscillatory Blowing, A Tool To Delay Separation, AIAA Journal, Vol. 31, No. 11, Pp. 2052-2060.

[11] **Wagner. R. D., And Fischer, M. C.,** 1984, Fresh Attack on Laminar Flow, Aerospace of America, Vol. 22, Pp. 72-76.

[12] **Karim, M. A., and Acharya**, 1994, M., Suppression of Dynamic-Stall Vortices Over Pitching Airfoils By Leading-Edge Suction, AIAA Journal Vol. 32, No. 8 Pp. 1647-1655.

[13] **Bayliss, A., Maestrello, L., Parikh, P., And Ting, L.,** 1986, Numerical Simulation of Boundary Layer Excition by Surface Heating or Cooling, AIAA Journal, Vol. 24, No. 7, Pp. 1096-1101.

[14] **Ahuja, K. K., Whipkey, R. R., And Jones, G. S., 1983,** Control Of Turbulent Boundary Layer Flows by Sound, AIAA Paper 83-0726.

[15] **Modi, V. J.**, 1997, Moving Surface Boundary Layer Control: A Review, Journal of Fluids and Structures, Vol. 11, Pp. 627-663.

[16] **Choi, S.,** Feb. 1998, The Active Control Of Boundary Layer Separation Via Periodic Buzzing On The Airfoil Surface, M.S. Thesis, Dept Of Mechanics And Aero Engineering, Seoul National Univ., Republic Of Korea.

[17] **Geissler, W, And Raffel, M,** Sept. 1993, Dynamic Stall Control By Airfoil Deformation, 19th European Rotorcraft Forum, Cernobio, Italy, Paper C2, 14-16.

[18] **Kehro, M, Hutcherson, S., Lieback, R,** Jan. 1990, Vortex Generators Used To Control Laminar Separation Bubbles, AIAA 90-0051.

[19] **C. Ramsey, J. L. Thomas, G. P. Warren And G. C. Liu,** 1986, Upwind Navier-Stokes Solutions For Periodic Flows, AIAA Paper 86-0247.

[20] **A. A. Hassan And R. D. Janakiram,** 1997, Effects Of Zero- Mass Synthetic Jets On The Aerodynamics Of The NACA-0012 Airfoil, AIAA 97-2326.

[21] **M.S. Chandrasekhara,** Oct. 1998, Unsteady Stall Control Using Dynamically Deforming Airfoils, AIAA Journal Vol. 36, No. 10.

[22] **Sahin M, Lakshmi N. Sankar, M.S., Chandrasekhara**, 2000, CHEE TUNG, Dynamic Stall Alleviation Using A Deformable Leading Edge Concept- A Numerical Study, In progress.

[23] **J. F. Donovan, Linda D. Kral and A. W. Carry**, 1998, Active Control Applied To An Airfoil, AIAA Paper 98-0210.

[24] **A. Seifert, T. Bachar, D. Koss, M. Shepshelovich And I. Wygnanski**, 31(11) 1993, Oscillatory Blowing: A Tool To Delay Boundary Layer Separation, AIAA Journal.

[25] **S. S. Ravindran**, December 1999, Active of Flow Separation Over an Airfoil" Nasa Langley Research Center Hampton, Virginia.

[26] **Karim M. A., Acharya M. And Metwally M. H,** Development of the Dynamic-Stall Vortex Over A Pitching Airfoil, Journal Of Fluid Mechanics.

[27] **Schlilting, H.** 1995, Boundary Layer Theory, Mcgraw Hill Book Company, New York.

[28] **Rott, N.** Unsteady Viscous Flow In The Vicinity Of a Stagnation Point, Quart. Appl. Math., Vol. 13, Pp 444-451.

[29] **Moore, F. K.**, 1958 On the Separation of the Unsteady Laminar Boundary Layer, IUTAM Symposium, Boundary Layers, H. Gortler, Ed., Pp 296-311.

[30] **Currier, J. And Fung, K-Y,** 1991**,** An Analysis Of The Onset Of Dynamic Stall, AIAA Paper No. 91-0003.

[31] **Mueller, T. J. And Batill, S. M**, 1982, Experimental Studies Of Separation On A Two-Dimensional Airfoil At Low Reynolds Numbers, AIAA J., Vol. 20, No. 4, Pp 457-463.

[32] **Lissaman**, 1983, Low-Reynolds Number Airfoils, Ann. Rev. Fluid Mechanics Vol. 15, Pp 223-239.

[33] **Lovato Julie Anne**, 1992, Active Control of the Separation Region on a 2-D Airfoil, Washington State, University Doctor of Philosophy.

BIOGRAPHY

First Lieutenant A. TUNC was born in August 02, 1977 in Ankara, Turkey. He had his elementary and secondary school education in the same place. Then, he was assigned to Maltepe Military High School, Izmir, Turkey. He graduated from Maltepe Military High School in 1995. After that, he received a Bachelor of Science degree in aeronautical engineering from the Turkish Air Force Academy, Istanbul, Turkey in August 30, 1999 and he graduated from Air Force Academy as a Second Lieutenant in the same date.

He received his intelligence officer training at Gaziemir Air staff Training Center, Izmir, Turkey from August 2000 through June 2001. He was assigned to the 143th Squadron, 4th Air Force Base, Ankara, in June 2001 as an intelligence officer. While working in this squadron, he was assigned to a special Masters of Science program that was organized by Istanbul Technical University, Istanbul, Turkey and Old Dominion University, Norfolk, VA., USA. He was promoted to first lieutenant in August 30, 2002.

.